TITLE
ASP Conference Series, Vol. **VOLUME***, **YEAR OF PUBLICATION**
NAMES OF EDITORS

Galaxy Formation Now and Then

Matthias Steinmetz

Astrophysikalisches Institut Potsdam, An der Sternwarte 16, 14482 Potsdam, Germany

Steward Observatory, University of Arizona, 933 N Cherry Ave, Tucson, AZ 85721, USA

Abstract.

I review the current state of our understanding of the galaxy formation and evolution process from the modeler's perspective. With the advent of the cold dark matter model and the support of fast computers and advanced simulation techniques, there has been considerable progress in explaining the growth of structure on the largest scales and in reproducing some of the basic properties of galaxies and their evolution with redshift. However, many properties of galaxies are still only poorly understood or appear to be in conflict with the prediction of the cold dark matter model. I discuss in what direction the next generation of galaxy formation models may go and why a large space-based optical-UV telescope could be critical for the calibration and testing of these advanced models.

1. Introduction

The past couple of years have witnessed a dramatic increase in the quantity and quality of observations on the formation and evolution of galaxies. Galaxies are routinely identified at redshifts exceeding three and high resolution imaging allows us to study their internal structure. These data are complemented by high resolution spectroscopy of QSO absorption systems that provide further clues on the evolution of baryons in the universe. In fact, this increase has been so rapid that observations have outgrown their theoretical framework. Traditional approaches, which rely heavily on the morphological classification of galaxies and which intend to disentangle the star formation history of galaxies, seem outdated if compared with the much richer structure seen in galaxies at different redshifts.

Motivated by the increasing body of evidence that most of the mass of the universe consist of invisible "dark" matter, and by the particle physicist's inference that this dark matter consists of exotic non-baryonic particles, a new and on the long run much more fruitful approach has been developed: rather than to model the formation and evolution of galaxies from properties of present day galaxies, it is attempted to prescribe a set of reasonable initial conditions. The evolution of galaxies is then modeled based on physical processes that are considered to be relevant such as gravity, hydrodynamics, radiative cooling and star formation. The outcome at different epochs is then confronted against

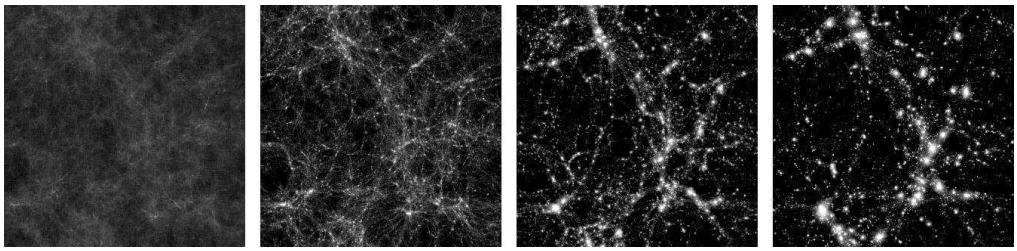

Figure 1. Time sequence of structure formation in a hierarchical clustering universe, here for the so-called ΛCDM model. The four snapshots correspond (from left to right) to redshifts of 9, 3.5, 1 and 0, respectively. The simulation box is 50 Mpc (comoving) on the side.

observational data. One scenario that has been extensively tested in this way is the model of hierarchical clustering, currently the most successful paradigm of structure formation.

In this contribution I review the main successes but also some of the generic problems of models in which structure forms by hierarchical clustering. I briefly compare the current state of the field with that 10-15 years ago followed by some speculations in which direction the field may develop in the next decade and how a large optical-UV telescope in space may support such developments.

2. The state of the field

Hierarchical clustering is at present the most successful model for structure formation in the universe. In this scenario, structure grows as objects of progressively larger mass merge and collapse to form newly virialized systems (Figure 1). Probably the best known representative of this class of models is the *Cold Dark Matter* (CDM) scenario. The initial conditions consist of the cosmological parameters $(\Omega, \Omega_{\rm baryon}, \Lambda, H_0)$ and of an initial density fluctuation spectrum such as the CDM spectrum. The remaining free parameter, the amplitude of these initial fluctuations, is calibrated by observational data, e.g., the measured anisotropies of the microwave background. Since the CDM model was introduced in the early 80s the values of these parameters have been revised and tuned to match an ever growing list of observational constraints, from the $\Omega_0 = 1$, $H_0 = 50\,{\rm km\ s^{-1}Mpc^{-1}}$, and $\sigma_8 = 0.6$ of the former "standard" Cold Dark Matter model to the currently popular "concordance" ΛCDM model. This ΛCDM model envisions an eternally expanding universe with the following properties (Bahcall et al. 1999): (i) matter makes up at present less than about a third of the critical density for closure ($\Omega_0 \approx 0.3$); (ii) a non-zero cosmological constant restores the flat geometry predicted by most inflationary models of the early universe ($\Lambda_0 = 1 - \Omega_0 \approx 0.7$); (iii) the present rate of universal expansion is $H_0 \approx 70$ km s^{-1} Mpc^{-1}; (iv) baryons make up a very small fraction of the mass of the universe ($\Omega_b \approx 0.04 \ll \Omega_0$); and (v) the present-day *rms* mass fluctuations on spheres of radius 8 h^{-1} Mpc is of order unity ($\sigma_8 \approx 0.9$). The hierarchical structure formation process in this ΛCDM scenario is illustrated in Figure 1, which depicts the growth of structure within a 50 Mpc box between

redshifts nine and zero. The ΛCDM model is consistent with an impressive array of well-established fundamental observations such as the age of the universe as measured from the oldest stars, the extragalactic distance scale as measured by distant Cepheids, the primordial abundance of the light elements, the baryonic mass fraction of galaxy clusters, the amplitude of the Cosmic Microwave Background fluctuations measured by COBE, BOOMERANG, MAXIMA and DASI, the present-day number density of massive galaxy clusters, the shape and amplitude of galaxy clustering patterns, the magnitude of large-scale coherent motions of galaxy systems, and the world geometry inferred from observations of distant type Ia supernovae, among others.

The hierarchical build-up is also thought to determine the morphology of a galaxy, most noticeably the difference between disk–like systems such as spiral galaxies (some of them barred) and spheroidal systems such as elliptical galaxies and bulges. This picture envisions that whenever gas is accreted in a smooth fashion, it settles in rotationally supported disk-like structures in which gas is slowly transformed into stars. Mergers, however, convert disks into spheroids. The Hubble type of a galaxy is thus determined by a continuing sequence of destruction of disks by mergers, accompanied by the formation of spheroidal systems, followed by the reassembly of disks due to smooth accretion (Figure 2). This picture of a hierarchical origin of galaxy morphology has been schematically incorporated in so-called semi-analytical galaxy formation models used to study the evolution of the galaxy population, but its validity in a cosmological setting has only just recently been directly demonstrated (Steinmetz & Navarro 2002).

Numerical simulations have been an integral part in the detailed analysis of the virtues of the CDM scenario. Only numerical techniques can account for the highly irregular structure formation process and for at least some of the complicated interaction between gravity and other relevant physical processes such as gas dynamical shocks, star formation and feedback processes. Simulations also provide the required interface to compare theoretical models with observational data and are able to link together different epochs. While simulations of structure formation on the larger scales have mainly used large massively parallel supercomputers, studies how individual structures such as galaxies or clusters of galaxies form in the ΛCDM scenario have heavily used special purpose hardware like the GRAPE (=GRAvity PipE) family of hardware N-body integrators (Sugimoto et al. 1990).

Although gas dynamical simulations were considerably successful in explaining some details of the galaxy formation process, the largest impact so far has been in the field of QSO absorption systems. Numerical simulations can reproduce the basic properties of QSO absorbers covering many orders of magnitude in column density (Cen et al. 1994; Zhang, Anninos & Norman 1995; Hernquist et al. 1996; Haehnelt, Steinmetz & Rauch 1996). Indeed, gas dynamical simulations were even responsible for a paradigm shift, as QSO absorbers are no longer considered to be caused by individual gas clouds. Absorbers of different column density (Ly-α forest, metal line systems, Lyman–limit systems and damped Ly-α absorption systems) are rather reflecting different aspects of the large-scale structure of the universe. While the lowest column density systems ($\log N \approx 12 - 14$) arises from gas in voids and sheets of the "cosmic web", sys-

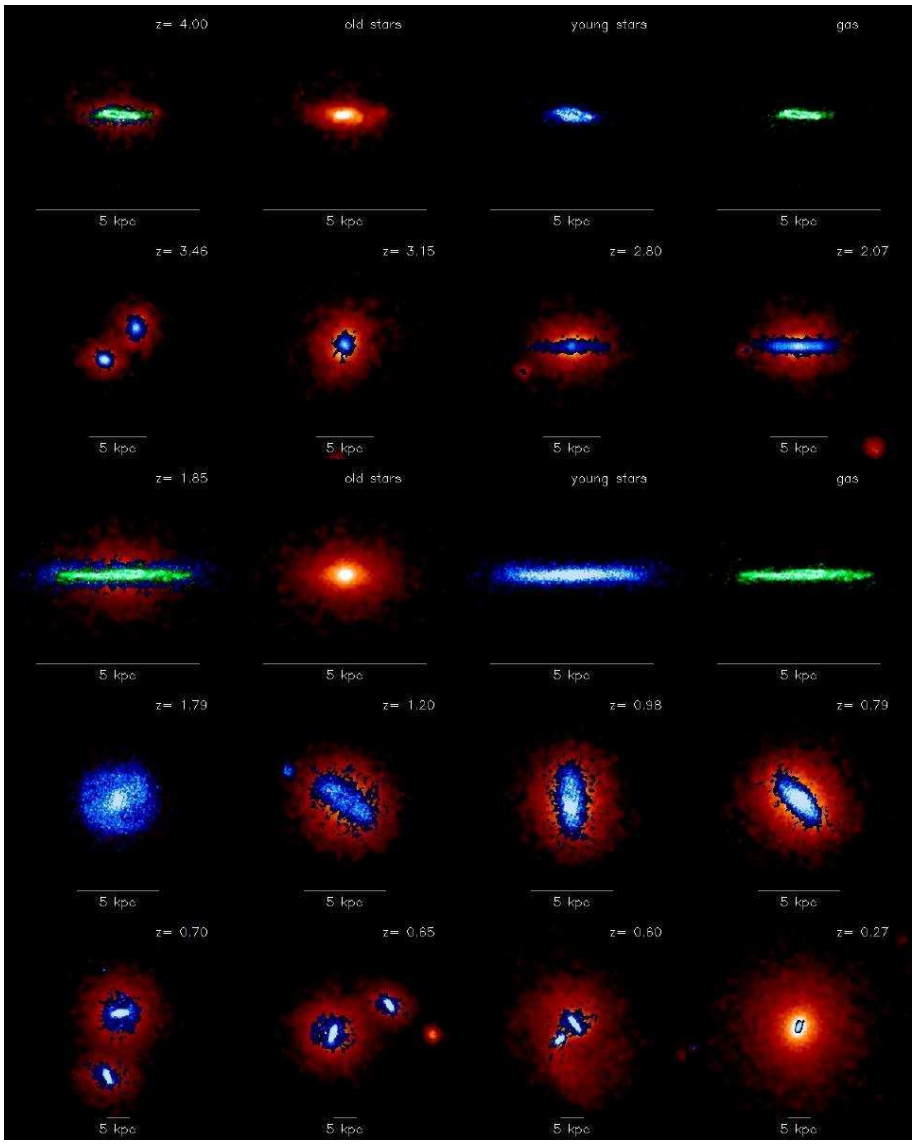

Figure 2. Surface mass density of the gaseous and stellar components of ΛCDM halo at various epochs. Horizontal bars in each panel are 5 (physical) kpc long and indicate the scale of each figure. Rows 2, 4 and 5 show time sequences near some key evolutionary stage. Rows 1 and 3 decompose a galaxy at a particular redshift (left) into its constituents: old stars, young stars and gas (from left to right). Top row: The most massive progenitor at z=4, seen edge-on. Second row: The formation of a bulge and the rebirth of a disk. Third row: The appearance of the galaxy at z=1.8, seen edge-on. Fourth row: The tidal triggering of bar instability by a satellite resulting in the emergence of a rapidly rotating bar. Bottom row: A major merger and the formation of an elliptical galaxy.

tems of higher column density are produced by filaments ($\log N \approx 14 - 17$) or even by gas that has cooled and collapsed in virialized halos ($\log N > 17$).

Even though the above list of achievements appears quite impressive, it mainly addresses structures on scales exceeding a few hundred kpc. On smaller scales, theoretical models have at best provided some qualitative insights in the physics of the galaxy formation process, but we are still far from being able to make quantitative predictions of the properties of the galaxies now or at higher redshifts on those small scales. For example, even though we have some qualitative insight how the Hubble sequence has formed, we are still unable to account in detail for the mix of morphologies at different redshifts. To a lesser extent we still do not have the computing power in order to study the small scale properties for a cosmologically representative sample of galaxies, but the more important factor is likely our rather poor understanding of the astrophysical processes acting on such scales such as star formation, and energetic feedback from supernovae and stellar winds.

Furthermore, a list of findings has surfaced in the past few years that seem to be at odds with the model predictions: (i) Because of their negligible primordial velocity dispersion, cold dark matter particles can achieve enormous phase space densities. As a result, numerical simulations have consistently shown that near the centers of halos the density profiles of virialized CDM halos diverge as r^{-1} (Navarro, Frenk & White 1996) or perhaps even as steeply as $r^{-3/2}$ (Moore et al. 1999a). These divergent profiles are at odds with the usual interpretation given to the "solid-body" HI rotation curves reported for some low surface brightness (LSB) dwarf galaxies (Flores and Primack 1994, Moore 1994). (ii) Another generic prediction of CDM models is that virialized galactic halos will typically be triaxial and have dense cores. Yet in a number of galaxies where detailed stellar and gas dynamical observations are possible, the dark matter contribution within the optical radius appears to be rather small: many disks, perhaps including the Milky Way, are "maximal" (see, e.g., Debattista & Selwood 1999). (iii) High resolution N-body simulations indicate that, if the dark halo of our own Milky Way is made up of CDM, it should contain several hundred dark matter sub-condensations; a number that climbs to roughly one thousand if all halos within the Local Group are considered (Klypin et al. 1999, Moore et al. 1999b). On the other hand, observations of the Milky Way surroundings and of the Local Group reveal an order of magnitude fewer galaxies than expected in this picture (Mateo 1998). (iv) A difficulty indirectly related to the substructure problem concerns the angular momentum of gaseous disks assembled in hierarchical clustering scenarios. In the absence of heating, most of the mass of a galactic disk forming within a CDM halo is accreted through mergers of proto galaxies whose own gas components have previously collapsed to form centrifugally supported disks. Numerical simulations (Navarro & Benz 1991, Navarro, Frenk & White 1995, Navarro & Steinmetz 1997) show that most of the angular momentum of the gas is transferred to the surrounding halos during mergers. As a result, the spin of gaseous disks formed by hierarchical mergers is much lower than those of observed spirals.

It should be clear from this list that a considerable concerted effort is required by the community in order to promote our cosmological concordance model to a concordance model of galaxy formation. Considering the complexity

of the processes involved, progress is likely to continue to be drive by observations.

3. Where did we come from ?

Before speculating what the state of the field may be like in 10–15 years, it may be illustrative to reconsider how the current state described above compares to the state of the field 10–15 years ago, i.e. before the advent of the Hubble Space Telescope and ground-based 8m class telescopes. Cosmological parameters were only very poorly constrained, the Hubble constant was known to only within a factor of 2, Ω at best to within a factor of ten. Hierarchical clustering in the form of a $\Omega = 1$ CDM model was already favored by most theorists, but it was certainly not accepted within the larger community as it is today. Similar statements can be made concerning the more basic concept that the morphological type of a galaxy may primarily reflect its merging history. From the observational side, barring some episodic evidence of very high redshift objects (radio galaxies, QSOs) and some indirect evidence for evolution (e.g. Butcher-Oemler effect), whose relationship to regular galaxies was quite unclear, galaxy properties were mainly determined only at very low redshift. In fact, most galaxy models did not, or if so only very schematically, include a cosmological context. Similarly, galaxy populations were mainly discussed in terms of non-evolution *vs* passive evolution models. It should be clear from this listing how rapidly the field of galaxy formation has changed in the past decade.

4. Prospects

Considering this rapid progress it seems (and probably is) impossible to make sound predictions how the field may change over the next ten or even fifteen years. Nevertheless, the exercise may be entertaining especially if one comes back for an evaluation after ten years. Assuming that the field continues to progress at the same pace and that basic concepts (like ΛCDM as a cosmological concordance model) remain unchanged, the following list appears to be "fair bets":

- Microwave background experiments, in particular satellite missions like MAP and PLANCK, will accurately determine the cosmological parameters. Extragalactic astronomy will therefore be dominated by the quest to understand the formation and evolution of galaxies and the astrophysics behind it, and will no longer be just a tool to measure cosmological parameters.

- The Next Generation Space Telescope (NGST) will provide us with a look at the so-called dark ages of the universe, i.e. the universe at redshift larger than six. Furthermore, NGST will allow us to study the evolution of the stellar component between redshift 3 and 1, the epoch in which galaxies appear to have developed from some irregular bright clumps into the Hubble sequence.

- Astrometric missions like GAIA will provide a detailed dynamical and chemical record of how the Milky Way has been built up and how it transformed its gas into stars.
- In ground-based astronomy, the second generation of instrumentation on 8m-class telescopes will be routinely used, and (from an optimist's point of view) first data may already come in from 30m optical telescopes.
- Galaxy formation models will largely benefit from the increase in computing power. According to Moore's law, the speed of computers doubles every 18 month. If this trend continues to hold, then standard PCs in 15 years will have a speed comparable to the largest supercomputers today. By then numerical simulation should be capable of simulating cosmologically representative volumes (a few hundred Mpc) of the universe at a resolution better than a kpc. The understanding of astrophysics rather than the availability of sufficient CPU power will limit our insight into the details of the galaxy formation process.

What will be the role of a 8m optical/UV space telescope in this framework ? Two potential applications that depend critically on the availability of large UV-sensitive instruments are:

- *Observe the development of the Hubble sequence.* Deep high-resolution imaging of UV dropout galaxies between redshift 3 and 1 will unravel the building blocks of typical L^* galaxies at the present day epoch. Furthermore the transition from clumps at $z \approx 3$ to Hubble-type galaxies at $z \approx 1$ can be observed. By low-resolution spectroscopy, the kinematics and thus the development of scaling relations like the fundamental plane or the Tully-Fisher relation can be investigated.
- *Create a 3D-map of the baryons in the universe between z=3 and z=0.* Using fainter QSOs (as obtained, e.g., by the Sloan Survey) as background sources, several patches of the night sky can be probed by many lines-of-sight. High-resolution spectroscopy of these background sources will map out the distribution of baryons in the IGM and eventually provide detailed 3D maps of the gas density, temperature, metallicity and ionization state. The current paradigm that galaxies preferentially form at the intersections of filaments in the cosmic web can be directly probed. Studies of the transverse proximity effect measure in detail the evolution of the cosmic UV background and thus on the reionziation history of the universe. Furthermore they can constrain the amount of beaming in the UV flux of QSOs.

Should these developments be accompanied by a corresponding increase in our understanding of how stars form, how they release energy to the ISM and thus how star formation interacts with the evolution of galaxies, we may indeed make a major step toward a standard model of galaxy formation by 2020.

References

Bahcall, N., Ostriker, J.P., Perlmutter, S., Steinhardt, P. 1999, *Science*, 284, 1481.

Cen, R., Miralda-Escudé, J., Ostriker, J.P., Rauch, M., 1994, ApJ , 437, 9.

Debattista, V.P., Sellwood, J. 1999, ApJ, 493, L5.

Flores, R.A., Primack, J.R., 1994, ApJ, 427, L1

Haehnelt, M., Steinmetz, M., Rauch, M., 1996, ApJ, 465, L95.

Hernquist, L., Katz, N., Weinberg, D.H., Miralda–Escude J., 1996, ApJ, 457, L51.

Klypin, A., Kravtsov, A.V., Valenzuela, O., Prada, F., 1999, ApJ, 552, 82.

Mateo, M., 1998, ARA&A, 36, 435

Moore, B., 1994, Nature, 370, 629.

Moore, B., Quinn, T., Governato, F., Stadel, J., Lake, G., 1999a, MNRAS, 310, 1147.

Moore, B., Ghigna, S., Governato, F., Lake, G., Quinn, T., Stadel, J., 1999b, ApJ, 524, L19.

Navarro, J.F., Benz W., 1991, ApJ, 380, 320.

Navarro, J.F., Frenk, C.S., White, S.D.M., 1995, MNRAS, 275, 56.

Navarro, J.F., Frenk, C.S., White, S.D.M., 1996, ApJ, 462, 563.

Navarro, J.F., Steinmetz, M., 1997, ApJ, 478, 13.

Steinmetz, M., Navarro, J.F., 2002, New Astronomy, 7/4, 155

Sugimoto, D., Chikada, Y., Makino, J., Ito, T., Ebisuzaki, T., Umemura, M., 1990 *Nature* **345** 33

Zhang, Y., Anninos, P., Norman, M.L., 1995, ApJ, 453, L57.

Formation and Evolution of Disk Galaxies

Joseph Silk
University of Oxford
Astrophysics, Denys Wilkinson Building,
Keble Road, Oxford OX1 3RH, UK

Abstract. I review several of the current issues in the theory of disk galaxy formation. There is still much to be done, observationally and theoretically, before we can expect to approach an understanding of disk galaxies that is reliable enough to make robust predictions about the high redshift universe.

Keywords: galaxy, disk, star formation

1. Introduction

There is a well-accepted prescription for the formation of disk galaxies. The dark matter context works well. Dark potential wells develop hierarchically and acquire angular momentum via tidal torques with neighbouring protohalos. Baryons cool and dissipate their gravitational potential energy, and conserve angular momentum to form a nearly self-gravitating disk of size λR_h, where λ is the dimensionless spin parameter acquired via nonlinear interactions and R_h is the halo virial radius. The disk cools and becomes gravitationally unstable to massive cloud formation. The clouds eventually themselves become unstable and fragment into stars that form a disk with an exponential surface brightness profile, a scale-length of a few kiloparsecs, and a central surface density of order hundreds of solar masses per square parsec for Milky-Way type spirals. Star formation, fed and self-regulated by disk instability, continues via ongoing accretion of gas into the disk from the halo reservoir of gas and small satellites.

There are numerous observational probes of this simple picture. The current star formation rate in disks is measured via $H\alpha$ emission, effectively probing the formation of massive stars. The disk gas fraction is measured via HI and CO observations, and provides the fuel that drives disk star formation. Multicolour imaging provides a measure of the spectral energy distribution, and probes the disk age over 10 Gyr. Stellar absorption features such as the Balmer spectral line index $H\beta$ measure ages over a baseline of about 2 Gyr. Large samples of disk galaxies, most recently utilizing the Sloan Digital Sky Survey, enable one to correlate surface brightness with total stellar mass, galaxy radii and colours. 21 cm and $H\alpha$ studies probe rotation curves, and allow

one to explore the Tully-Fisher relation. Galaxy scales, metallicities and correlations provide fossilized glimpses of the galaxy formation epoch. Observations at high redshift can directly target the epoch of formation. All of these probes lead to strong constraints on the basic disk formation model.

Theory provides a well-accepted framework for the hierarchical formation of dark matter halos. However it is far weaker when it comes to the formation and evolution of the star-forming components of galaxies. In this review, I will concentrate on disk galaxies, and discuss the problems that have arisen with some of the proposed solutions. Much of our understanding centres on the concept of self-regulation of the global star formation rate. Unfortunately, some of the key ingredients are poorly known.

2. Disk formation

The dark matter that dominates the matter budget of the universe, and in particular the galactic mass budget, is considered to be non-dissipative. While the precise nature of the dark matter remains elusive, the hierarchical formation of non-dissipative dark potential wells in which baryons dissipate and condense into stars, has provided a successful model for many elements of the large-scale structure of the galaxy distribution (White & Rees, 1978). Galaxy clustering can be explained in such a framework, as can the properties of the dark halos that are inferred, for example, from rotation curves, and of the intergalactic medium where neutral baryons in the form of the Lyman alpha forest provide a powerful probe of the weakly nonlinear regime. Tidal torques are generated by nonlinear interactions between neighbouring fluctuations and nascent halos. If the baryons conserve angular momentum as they dissipate kinetic energy and contract, disks spanning the observed size distribution are formed. The distribution of angular momentum is not such a good match, as the theory predicts far more low angular momentum gas than is seen. Once the baryon disk is self-gravitating, it is gravitationally unstable and fragments into stars. This general overview of disk formation can match many of the observed properties of disks provided that disk star formation is an inefficient process. Observed disks are still gas-rich and star formation extends over 50 or more disk dynamical time-scales.

3. Global star formation in disks

Disk star formation can be understood via a hybrid model that is a combination of phenomenology and gravitational instability theory. The low efficiency of star formation is determined by the gravitational instability of a cold gas-rich disk, resulting in the formation of warm molecular gas clouds which in turn fragment into stars. Cloud collapse and star formation are enhanced by cloud coalescence and growth, as the clouds orbit the galaxy. This process is modulated and amplified by the spiral density wave pattern of the differentially rotating disk. The instability in a gas disk is quenched by the Toomre criterion, when the Toomre parameter, $Q \equiv \mu_{crit}/\mu_{gas}$, becomes larger than unity. Here the critical surface density is, to within a numerical factor of order unity, given by $\kappa\sigma_{gas}/G$ with κ equal to the epicyclic frequency and σ_{gas} being the gas velocity dispersion. For a disk consisting of stars and gas, the criterion must be slightly modified, but it is essentially the coldest component, the gas, that drives the instability, provided that the gas surface density $\mu_{gas} \gtrsim \mu_*\sigma_g/\sigma_*$, where μ_* is the disk stellar surface density and σ_* is the stellar velocity dispersion.

This scheme is used to derive an empirical star formation rate, the Schmidt-Kennicutt law, which has been applied to fit a large sample of star-forming disk galaxies. Beyond the radius where the azimuthally-averaged surface density drops below the critical value, the disk is stable to cloud formation. The inferred star formation rate, if one assumes that the clouds once formed are unstable to star formation within a disk rotation time or less, can be approximated by

$$\dot{\mu}_* = \epsilon\mu_{gas}^n\Omega(Q^{-2} - 1),$$

for $Q < 1$, with $n \approx 1$. The instability requires the disk to be in differential rotation, at rate $\Omega(r)$.

The predictions of such a semi-empirical model are straightforward: star formation occurs inside-out in disks, quenching below the threshold surface density of cold gas (HI or H_2) of a few solar masses per square parsec, and star formation decays monotonically as the gas supply is exhausted. The duration of star formation can be extended if gas infall occurs from the halo.

Broadly viewed, such a model works reasonably well from the point of view of chemical evolution (cf. Prantzos, these proceedings). However detailed recent studies of disk star formation suggest that there are significant omissions in the underlying physics. For example, there is the realization that the radial dependence of disk star formation is not always well modeled by the empirical law (Ferguson et al., 1998). In some galaxies, star formation occurs below the threshold surface den-

sity. This is most likely due to the non-axially symmetric distribution of the gas. Locally the gas surface density may be high, as for example in spiral arms.

Another hint of the need for a more complex theory comes from studies of the age distribution of disk stars. In the Milky Way, the star formation rate history is seen to be non-monotonic (Rocha-Pinto et al., 2000). In fact, studies of chromospheric age indicators reveal a series of modest star bursts. A similar pattern is found in other nearby galaxies where stars can be resolved, and the Hertzsprung-Russell diagram can be used to study the star formation history. Presumably, infall is occurring in a non-uniform way, for example via mergers of satellite galaxies. Studies of the metallicity distribution of old disk stars in the solar neighbourhood require early infall in order to account for the paucity of old metal-poor stars.

The underlying logic of dissipative disk formation in weakly interacting halos of cold dark matter seems compelling. Star formation is inefficient in disks because of self-regulation. The disk forms via collapse in the dark halo of gas that has acquired some angular momentum via tidal torques between neighbouring halos. The dimensionless angular momentum parameter is initially $v_{rot}/\sigma \approx 0.15$, and contraction by a factor of order 10 in an isothermal dark halo of virial radius 100 kpc that dominates the gravity results in a disk of scale around 5 kpc if specific angular momentum is approximately conserved.

The gas disk is cold and gravitationally unstable, forming giant cloud complexes that aggregate gas and are in turn unstable to fragmentation. Feedback both via dynamical heating of the stars and by supernova remnant interactions heat and stabilize the system against further star formation, until further gas infall drives further gas cooling.

Because of the bottom-up nature of the clustering hierarchy, driven by the approximately scale-invariant primordial density fluctuation spectrum, the density fluctuation amplitude scales with mass as $\delta\rho/\rho \propto (1+z)^{-1}M^{-(n+3)/6}$ with $n \approx -1.5$ on galaxy scales. This means that massive halos form after lower mass halos, with the virialization redshift scaling as approximately $M^{-1/4}$. There is as much mass in the low mass halos as in the massive halos, with the number of halos scaling as $dN/dM \propto M^{-2}$.

There are serious deficiencies in the model that remain when disk formation is incorporated by such simple rules into semi-analytic galaxy formation theory that builds on numerical simulations of dark matter clusters.

4. The dark side of disk formation

Several fundamental problems have arisen in detailed attempts to implement disk formation. The baryons undergo excessive cooling. The highest resolution simulations to date have revealed that as a consequence of the unresolved clumpiness of the dark matter, most of the baryonic angular momentum is lost to the dark halo by dynamical friction of infalling baryon clumps. The final specific angular momentum is only twenty percent or less of what is observed. The angular momentum distribution also does not match that of dark halos if the baryon angular momentum distribution tracks that of the dark matter, there being far too much low angular momentum gas at small galactocentric radii in the models. Even if angular momentum is assumed to be conserved by the baryons, the final disk in a Milky Way-like galaxy is about twice as massive as observed.

One issue is generic to hierarchical formation models with a specified efficiency of turning gas into stars. The most massive systems form late, and hence are expected to be younger and therefore bluer than less massive disks. The opposite trend is seen in the disk colour-magnitude relation (van den Bosch, 2002).

A further difficulty arises from the substructure in the dark halos that results in the formation of many satellite halos. These are not observed as stellar systems, for example in the distribution of Local Group dwarf galaxies. Another problem concerns the density distribution of the dark matter halos. The dark matter halos seem to be too concentrated compared to actual galaxies. Cusps are predicted in the halo cores that are not seen in nature, and the ratio of dark mass to baryonic mass is excessive in the vicinity of the baryon-dominated disk.

Several galaxies have been modelled in detail and illustrate these various trends. The Milky Way has the best studied rotation curve. Binney and Evans combined the inner rotation curve with microlensing data to infer that the observed microlensing optical depth towards the galactic centre requires so many stars that one has difficulty in acommodating a diffuse cold dark matter component. No more than 10 percent of the dark matter within 5 kpc can be diffuse and non-baryonic (Binney & Evans, 2001). In particular, the NFW profile ($\rho \propto r^{-1}$ for $r < r_s$ with $r_s \sim 0.1 r_{200}$) is not allowed. Indeed, the highest resolution simulations require an even steeper dark matter cusp; $\rho \propto r^{-1.5}$. This certainly would not allow enough bulge and inner disk stars to give a reasonable microlensing optical depth.

A complementary study by Klypin et al focuses on the outer Milky Way rotation curve. They argue that up to half of the mass within 10 kpc may be contributed by the dark halo, thereby allowing a NFW

profile (Klypin, Zhao and Somerville, 2002). However this conclusion comes at a cost. Only 60 percent of the baryons inferred by the model to be within the virial radius can be accomodated in the bulge, stellar halo and disk, including interstellar matter. Most of the observed mass of course is in stars, which are measured directly for stars of order a solar mass or larger, and via rotation curve modelling, diffuse infrared emission and bulge microlensing for the least massive stars. All disk formation and evolution simulations seem to run into a similar difficulty, as for example in a recent discussion of colour evolution (Westera et al., 2002).

Several of these issues are manifestations of the overcooling problem that is generic to hierarchical structure formation models. The cooled baryon fraction in cluster simulations is about 30 percent, whereas the global CDM prediction is about 5 percent for the baryon fraction, which for $\Omega_m \approx 0.3$ predicts 15 percent for rich clusters, as indeed is observed. About half of the cooled baryons remain on the peripheries of clusters as the warm/hot intergalactic medium at $T \sim 10^5 - 10^6$ K. Numerical SPH simulations find such a WIGM, although the physics of how this gas is heated yet remains outside the cluster virial radius is not completely clear. Shock heating is obviously important, but there are numerical issues that need to be clarified. The WIGM however only acccounts for about 30 percent of the total baryon content of the low redshift universe. The cluster x-ray luminosity-temperature correlation, which monitors the mass in virialised gas, does not satisfy the simple scaling expected in hierarchical collapse models, but rather suggests that preheating, preferentially in the lower mass clusters, may have helped to steepen the luminosity-temperature correlation from $L_x \stackrel{\propto}{\sim} T^2$ to $L_x \stackrel{\propto}{\sim} T^2$.

Another probe of dark matter in reasonably luminous disks comes from studying the kinematics of barred galaxies. Debattista and Sellwood argued that a maximal disk is required, eg for NGC 3198, in order to maintain a self-gravitating bar (Debattista & Sellwood, 2000). On the other hand, Kranz et al. find varying results for the disk mass fraction by modelling the detailed kinematic structure, for example the (unbarred) galaxy NGC 4254 requires a submaximal disk (Kranz, Slyz and Rix, 2002).

The colour-magnitude relation (B-K versus K) reveals another difficulty (van den Bosch, 2002). The more luminous galaxies, the redder they are, indicative of less vigorous recent star formation. SEmi-analytical disk models, even when feedback is included, give the inverse correlation. This is another manifestation of the overcooling problem. The oldest early-type galaxies are found to be the most massive, and these have the highest $[\alpha/Fe]$, indicative of the shortest star forma-

tion time-scales. The opposite trend is expected in hierarchical models (Thomas, Maraston and Bender, 2002).

5. Proposed solutions

The baryon fraction in stars may be understood if approximately half the baryons that initially cooled within the virial radius have been expelled. Supernova feedback seems incapable of driving such a wind in the early gas-rich phase of galaxy formation because of the significance of cooling. However there are indications that vigorous winds are seen in the Lyman break galaxies, as inferred from the inverse P Cygni line profiles in template spectra and from the Lyman alpha forest suppression found within a Mpc or so of the Lyman break galaxies. In nearby galaxies where so-called superwinds are found, the observed mass outflow rate is comparable to the star formation rate, e.g. in NGC 253 (Strickland et al., 2002). Observations suggest that strong winds can be driven from typical galaxies, yet numerical simulations find that winds are stalled for the more massive halos.

What physics has hitherto been omitted from the simulations? The simulations are gravity-driven. Star formation may be, in extreme situations, pressure-driven. This could result in strong positive feedback via for example shock-triggered massive star formation and generate enhanced rates of correlated supernovae. that would in turn drive a transient wind.

Starbursts are known to drive winds. One mechanism appeals to bar formation. A merger creates a transient bar. The spin-down and dissolution of this bar torques and accelerates the gas which responds by an enhanced rate of dissipation and angular momentum loss, for example via cloud-cloud collisions. Bars are known to drive luminous starbursts, and minor mergers may drive ultraluminous starbursts, the ultimate sources of superwinds.

The gas-rich environment provides a plausible site for supermassive black hole formation. This phenomenon appears to occur contemporaneously with spheroid formation, as inferred from the remarkable correlation between central black hole mass and spheroid velocity dispersion. SMBH-driven outflows, manifest as a SMBH-energized component of the overall luminosity, may be important in early phases of galaxy formation. At least one explanation of the observed correlation appeals to outflows as the self-regulatory mechanism.

While the formation of structure in halos building up from clouds of weakly interacting dark matter is reasonably well understood, the formation of the luminous components of galaxies is founded on sim-

plistic assumptions. A more realistic treatment of star formation in forming galaxies must ultimately modify many of the predictions that are failing to adequately confront the observations.

Feedback from supernovae is one solution that is being widely discussed. Supernova remnants deposit substantial energy into the interstellar medium, and are responsible for the observed multiphase structure of the interstellar gas. Some nearby low mass star-forming galaxies show a porous structure in the interstellar gas, where many overlapping shells and bubbles are seen that demonstrate that supernova input is playing an important role in pressurizing the interstellar gas. Some display an anti-correlation between X-ray and $H\alpha$ emission, indicative of supernova-driven bubbles. The microphysics of the interface between the supernova-heated gas and the cold interstellar medium is inadequately resolved by the simulations. Plausibly, there are surprises in store.

Feedback reduces the efficiency of star formation. This is important for understanding the longevity of disk star formation. However attempts to use feedback in the phase of disk formation have had mixed success. A basic problem is that feedback delays star formation: if this works too well, all stars are young, in contrast to what is found in the outer parts of nearby disks such as M31. Numerical simulations that incorporate feedback find that disks are still too small, although possibly by only a factor of 2 (Sommer-Larsen, Gotz and Portinari, 2002).

If efficiency of star formation is to account for the observed colour-magnitude relation, then one needs a systematic reduction in efficiency of star formation with decreasing galaxy mass. Some evidence for this is found in the correlations between stellar surface brightness and total stellar mass in the SDSS study of 80,000 early and late-type galaxies (Kauffmann et al., 2002). In ellipticals, such an effect would help to simultaneously account for the trend of increasing $[\alpha/Fe]$ with galaxy mass, if the most massive galaxies are the oldest and formed stars most rapidly. However no detailed implementation has been made of the relevant physics, in large part because one needs to incorporate a multiphase interstellar medium.

6. Analytic disk galaxy formation

The brute force computational approach will not resolve the outstanding problems in disk galaxy formation. What seems to be needed are further analytical insights that will allow refinement of the simple prescriptions for star formation. One such approach has come from

studying turbulence-driven viscous evolution of differentially rotating disks. Recent investigations of star formation suggest that turbulence plays an important role in accounting for the longevity of star-forming clouds and their fragmentation into stars. The Jeans mass in a typical interstellar cloud greatly exceeds the stellar mass range. It is likely that the gravitational instability of galaxy disks is a primary source of interstellar cloud turbulent motions, supplemented on small scales by supernova feedback. Of course, these drivers of turbulence are coupled together, since the rates of star formation and star deaths are controlled by global gravitational instability. In effect, differential rotation is the ultimate source of the turbulence.

A promising hypothesis is that turbulent viscosity, by regulating the gas flow, controls the star formation rate, and indeed that the star formation time-scale is given by the time-scale for the viscous transfer of angular momentum (Silk and Norman, 1981). On the scale of molecular clouds, such an ansatz is reasonable, since one has to shed angular momentum in order to form stars. Magnetic fields are the common culprit in conventional star-forming clouds, but in protogalactic disks one most likely has to appeal to another source of angular momentum transfer. Turbulent viscosity is capable of fulfilling this role. Indeed, the resulting disk has been shown to generically develop an exponential density profile (Lin and Pringle, 1987). In infall models, the initial angular momentum profile determines the final disk scale length if angular momentum is conserved. However as found in high resolution simulations, some 90 percent of the baryonic specific angular momentum is lost to the dark halo, and there is no preferred solution for disk sizes. In viscous disk models, the scale length is set by the competition between viscosity-driven star formation, that freezes the scale length once stars form, and dynamical friction on the dark matter, that competes for the same angular momentum supply. The characteristic viscous scale is determined by the cloud mean free path between collisions, itself comparable to the disk instability scale that drives the turbulence, and in combination with the residual rotation rate, provides the ultimate constraint on disk scales.

Another byproduct of the viscous disk model is the gas fraction (Silk, 2001). The viscous redistribution time-scale, and hence the star formation time-scale, is

$$t_\nu \approx t_{sf} \approx r_d^2/\sigma_{gas}\ell,$$

where ℓ is the cloud mean free path (of order the disk scale height), and σ_{gas} is the cloud velocity dispersion. Disk instability yields $\sigma_{gas} \approx \Omega\ell$. The star formation efficiency, if determined by supernova feedback and approximate conservation of momentum, is $\epsilon \approx \sigma_{gas}/v_{SN}$, where

v_{SN} is the specific supernova momentum per unit mass injected into the interstellar medium. Here $v_{SN} \equiv E_{SN}/m_{SN}v_c$, where m_{SN} is the mass in stars per supernova and v_c is the velocity of transition of a remnant to approximate momentum conservation. The characteristic star formation time may then defined to be

$$t_{sf} \approx \frac{M_*}{\dot{M}_*} \approx \frac{M_*}{\dot{M}_{gas}} \epsilon^{-1} \Omega^{-1},$$

where $\Omega(r)$ is the disk rotation rate at radius r, $M_*(r)$ is the instantaneous stellar mass and M_{gas} is the gas mass. A steady state is reached in which the gas fraction is

$$\frac{M_*}{M_{gas}} \approx \frac{\sigma_{gas} v_{SN}}{v_{rot}^2},$$

and the disk scale length is

$$r_d = \ell \sqrt{\Omega t_{sf}}.$$

Thus the disc scale depends both on cosmology and on local conditions.

The inferred present epoch numbers are plausible: for $M_* \approx 6 \times 10^{10} \mathrm{M}_\odot$, one finds $\dot{M}_* \approx 3 \mathrm{M}_\odot/\mathrm{yr}$ and $M_{gas}/M_* \approx 0.1$. Also, one has now $\sigma_{gas} \approx 10 \mathrm{kms}^{-1}$, $v_{SN} \approx 1000 \mathrm{kms}^{-1}$, and $\ell \approx 0.3$kpc. At disk formation, one expects that $M_{gas}/M_* \approx 1$, $t_{sf} \approx 10^9$ yr, and $\ell \approx 1$ kpc, appropriate to the protodisk. These values result in a stellar disk scale-length $r_d \approx 3$ kpc. It is encouraging that simple analytic estimates come out with reasonable numbers for gas and stellar disk scales and gas fraction. Whether such a simple model survives incorporation into 3-dimensional simulations of disk formation in the presence of a live dark matter halo and energetic winds remains of course to be seen.

7. Spheroid formation

Spheroids are an integral component of practically all disk galaxies. Studies of spheroid formation are complicated by the fact that there is no global theory of star formation even at the semi-empirical level that works moderately well for cold gas disks.

Small spheroids most likely form by secular evolution of bar-unstable disks. However it is not possible to form massive spheroids by secular evolution. Galaxy mergers are undoubtedly the major trigger for formation both of massive spheroids in early-type disk galaxies and of elliptical galaxies. It has been realized from the earliest simulations of mergers that gas-rich precursors are required in order to attain the

high central densities of massive spheroids. The gas dissipates, forms stars that in turn self-enrich more gas, ending up with the metal-rich nuclei characteristic of massive ellipticals. This must have happened with high efficiency, since spheroidal stellar populations are characteristically old. The necessarily high star formation rate constitutes a star burst, defined simply by the requirement that the mean star formation rate is inferred to have been much higher, perhaps by two orders of magnitude, than the mass of stars divided by a Hubble time.

Nearby starbursts are well studied. Typically, starbursts are rare in the nearby universe but increasingly common at high redshift. Star formation rates of up to 1000 $M_\odot$ yr^{-1} are inferred. The most extreme star formation rates are invariably associated with evidence for an ongoing merger. Most of the star formation generated by gas concentration triggered in a merger is shrouded by dust, and most of the radiation is absorbed and reemitted in the far infrared. Simulations demonstrate that the mergers of gas-rich galaxies efficiently drive the gas into the central kiloparsec of the merged galaxy by a powerful combination of tidal torquing on the gas due to the merged transient stellar bar that results from the merger, which removes angular momentum and compresses the gas, followed by strong dissipation of energy by radiative cooling of the gas.

Ultraluminous infrared starbursts are likely to be the sites of ongoing spheroid formation. This conjecture is supported by near-infrared observations of post-starburst galaxies, where the characteristic de Vaucouleurs profiles found in spheroids can be recognized in the newly formed stars.

There is an intriguing complication. Spheroids have been found to be intimately linked with supermassive black holes. The tight correlation observed between black hole mass and spheroid velocity dispersion covers the range of black hole masses 10^6 to 10^9 $M_\odot$. and encompasses stellar spheroids as small as that of the Milky Way ($\sim 10^9$ $M_\odot$) to those as massive as M87 ($\sim 10^{12}$ $M_\odot$). The clear implication is that the formation of spheroids and supermassive black holes was contemporaneous. If the spheroid formed by a merger, the strong central gas enhancement provides an ideal environment for supermassive black hole formation. The enormous amount of binding energy released as the SMBH formed would impact the protogalactic gaseous environment, as would the ensuing effects of energy released by infall into the newly formed black hole. Outflows would be a natural outcome, and these could help stimulate further star formation.

Observationally, it is unclear what role quasar-like activity plays in the energetics of the far-infrared and submillimeter galaxies that are undergoing luminous starbursts. In the nearby case of Arp 220, it is

apparent that star formation and buried quasars play comparable roles in accounting for the observed luminosity.

8. Conclusions

There seem to be two distinct modes of global star formation. An inefficient, quiescent mode that is self-regulated by feedback occurs in galactic disks. A violent, efficient starburst mode is triggered and fueled by merger-induced tidal torques, and accounts for the formation of the massive stellar spheroids. The disk mode of star formation most likely also accounts for the low mass spheroids, which are generated dynamically via secular evolution of disks.

Semi-analytic galaxy formation modelling has not yet incorporated the full richness of star formation phenomenology. There are five critical issues currently confronting semi-analytic theory, and improvements in star formation modelling and the dynamical coupling of baryonic and non-baryonic matter will be necessary to address most of them.

- Perhaps the most innocuous of the problems is the overproduction of substructure, and in particular the predicted abundance of dwarf galaxies. This is likely to be resolved at least in part by early photo-ionization at redshifts above 6, before the reionization of the intergalactic medium was complete. Early photo-ionization of dwarfs with velocity dispersion less than about 30 km/s suffices to eject most of the gas before the bulk of the star formation has occurred. Because this happens early, there is a proximity effect: only the most widely separated dwarfs, which experience a lower UV flux, retain their gas and survive as stellar systems. One can both account for the paucity of observed dwarfs and their mean separations from the parent galaxies. What is not yet clear is whether the number of SMC-like systems predicted is consistant with observations, nor more seriously perhaps, is whether reconciling the low dwarf abundance in the Local Group allows one to also understand the apparent surfeit of dwarfs observed in some nearby galaxy clusters.

- The baryon overcooling problem is more serious. The factor of about 2 excess predicted for disk baryons can be resolved either by ejection or by hiding the gas. Winds can occur if outflows from massive galaxies are stronger than predicted by simple disk modelling and simulations. The Lyman break galaxies possibly indicate the effectiveness of early winds, but it is likely that these galaxies end up as E or S0 galaxies, as inferred from their spatial clustering.

Substantial amounts of gas could be hidden in the form of dense cold clumps of H_2, or even in diffuse H_2 in the outer disk, where H_2 may be more readily hidden.

– Disk scale lengths can possibly be explained via turbulent feedback. Winds may play a role here too, if the predominantly low angular momentum gas, which ends up in the central core, is preferentially expelled. A supermassive black hole-driven outflow may provide a possible driver for the nuclear wind.

– Disk colours, and indeed spheroid colours, present another difficulty, as exemplified by the colour-magnitude relation. Disks, whose global colours are characteristic of intermediate age populations, have stellar populations that are systematically too red, and too old, at large masses. For ellipticals, the problem is somewhat different. The colour-magnitude relation is driven primarily by metallicity, with there being little evidence for any significant age spread in cluster galaxies (Vazdekis et al., 2001). The stellar populations are predominantly old. Both massive and low mass ellipticals have similar ages. Either the low mass systems formed stars earlier but less efficiently, hence reducing their effective age, or gas accretion occurred to produce a similar effect. The alpha element ratio enhancement for the cores of massive ellipticals supports an early and efficient duration of star formation for these systems. Field ellipticals and S0s however show a substantial age spread.

– The issue of a cusp in the dark matter profile represents a contentious issue around which the observations have not yet converged. It may be that dynamical effects, such as black hole mergers, provide the best means of scouring out the cusp. The related matter of dark matter concentration seems to vary between galaxies, and there are hints that it varies between barred and unbarred galaxies. This suggests again that a complex dynamical history may be partly to blame.

9. Acknowledgements

I am indebted to my group at Oxford for many discussions of galaxy formation, and in particular for conversations pertinent to this review with Julien Devriendt, Ignacio Ferreras, Adrianne Slyz and James Taylor. Part of this review was completed at the Institut d'Astrophysique

de Paris, where I am grateful to the Director, Bernard Fort, for his kind hospitality. I also thank N. Prantzos for useful discussions.

References

Binney, J. and Evans, N. 2001, MNRAS, 327, L27.
Debattista, V. and Sellwood, G. 2000, ApJ, 543, 704.
Ferguson, A., Wyse, R., Gallagher, J. and Hunter, D. 1998, ApJ, 506, L19.
Kauffmann, G. et al. 2002, astro-ph/0205070.
Klypin, A., Zhao, H. and Somerville, R. 2002, ApJ, 573, 597.
Kranz, T., Slyz, A. and Rix, H. 2001, ApJ, 562, 164.
Lin, D. and Pringle, J. 1987, ApJ, 320, 87L.
Rocha-Pinto, H., Scalo, J., Maciel, W. and Flynn, C. 2000, A&A, 358, 869.
Silk, J. 2001, MNRAS, 324, 313.
Silk, J. and Norman, C. 1981, ApJ, 247, 59.
Sommer-Larsen, J., Gotz, M. and Portinari, L. 2002, astro-ph/0204366.
Strickland, D. et al. 2002, ApJ, 568, 689.
Thomas, D., Maraston, C. and Bender, R. 2002, astro-ph/0202166
van den Bosch, F. 2002, MNRAS, 332, 456.
Vazdekis, A. et al. 2001, Ap.J., 551, L127.
Westera, P., Samlund, M., Buser, R. and Gerhard, O. 2002, A&A, submitted.
White, S. and Rees, M. 1978, MNRAS, 183, 341.

THE ASTROPHYSICAL JOURNAL, 562:593–604, 2001 December 1

DIRECT DETECTION OF WARM DARK MATTER IN THE X-RAY

KEVORK ABAZAJIAN,[1] GEORGE M. FULLER,[1] AND WALLACE H. TUCKER[1,2]

Received 2001 May 31; accepted 2001 July 31

ABSTRACT

We point out a serendipitous link between warm dark matter (WDM) models for structure formation on the one hand and the high-sensitivity energy range (1–10 keV) for X-ray photon detection on the *Chandra* and *XMM-Newton* observatories on the other. This fortuitous match may provide either a direct detection of the dark matter or the exclusion of many candidates. We estimate expected X-ray fluxes from field galaxies and clusters of galaxies if the dark matter halos of these objects are composed of WDM candidate particles with rest masses in the structure formation–preferred range (~ 1 to ~ 20 keV) and with small radiative decay branches. Existing observations lead us to conclude that for singlet neutrinos (possessing a very small mixing with active neutrinos) to be a viable WDM candidate they must have rest masses $\lesssim 5$ keV in the zero lepton number production mode. Future deeper observations may detect or exclude the entire parameter range for the zero lepton number case, perhaps restricting the viability of singlet neutrino WDM models to those where singlet production is driven by a significant lepton number. The Constellation X project has the capability to detect/exclude singlet neutrino WDM for lepton number values up to 10% of the photon number. We also consider diffuse X-ray background constraints on these scenarios. These same X-ray observations additionally may constrain parameters of active neutrino and gravitino WDM candidates.

Subject headings: dark matter — elementary particles — neutrinos — X-rays: diffuse background — X-rays: galaxies — X-rays: galaxies: clusters

1. INTRODUCTION

In this paper we show how the *Chandra*, *XMM-Newton*, and future Constellation X observatories can detect or exclude several warm dark matter (WDM) candidates, including singlet ("sterile") neutrinos, heavy active neutrinos, and gravitinos in some models. In essence, we show here how the technology of modern X-ray astronomy allows the exploration of a new sector of particle physics, one where interaction strengths could be characteristically some 10 orders of magnitude weaker than the weak interaction. Processes with these interaction strengths likely never could be probed directly in a laboratory.

The X-ray observatories, however, possess several advantages when it comes to probing WDM candidate particles. First, the sensitive energy range for X-ray photon detection on these instruments is ~ 1 to ~ 10 keV. Serendipitously, this is more or less coincident with the WDM candidate particle rest mass range that is preferred in studies of structure formation (Bode, Ostriker, & Turok 2001). Some models posit the production of WDM particles through their tiny interactions with ordinary matter. In several cases these very weak interactions lead to small radiative decay branches, producing photons with energies of order the WDM particle rest mass.

This is where the second advantage of X-ray astronomy comes in. Even though the WDM particle decay rate into photons can be very small (lifetimes against radiative decay are typically $\sim 10^{16} \times$ Hubble time), the dark matter halos of galaxies and galaxy clusters can contain huge numbers of particles, e.g., in the latter class of objects, some 10^{79} particles of rest mass ~ 1 keV. In effect, dark matter halos can serve as laboratories of enormous "fiducial volumes" of dark matter particles.

The first evidence for dark matter was the velocity dispersion of galaxies in the Coma Cluster, which required mass-to-light ratios in the cluster to exceed those inferred for our Galaxy by many times (Zwicky 1933). Later, observations of giant spiral galaxies implied that their disks are imbedded in larger halos of dark matter (Ostriker, Peebles, & Yahil 1974; Einasto, Kaasik, & Saar 1974). Recently, problems in cosmological structure formation models have led to interest in alternatives to the standard cold dark matter (CDM) model for structure formation.

The primary problem encountered in comparing calculations of structure formation in CDM models to observation is that simulations predict a large overabundance of small halos near galaxies such as our own. Structure formation in these models occurs through hierarchical growth of fragments into larger objects. This hierarchical structure is obvious in clusters of galaxies, where the numerous constituent galaxies are seen directly. Individual galaxy formation is also hierarchical in CDM simulations. These simulations predict a large number of dark matter subhalos, about 500, for each Milky Way–type halo (Moore et al. 1999; Ghigna et al. 2000); however, only 11 dwarf galaxies are observed near our Galaxy. The observed paucity of such substructure (dwarf galaxies) has been interpreted as a fundamental failure of CDM models. The hallmark of *cold* dark matter particles is a very small collisionless damping (free streaming) scale, i.e., considerably smaller than the scale associated with dwarf galaxies, ~ 0.3 Mpc ($\sim 10^{10}\ M_\odot$). Between the large free-streaming scale "top-down" hot dark matter (HDM) structure formation scenarios and the "bottom-up" scenarios of CDM models lies the intermediate regime of WDM (Colombi, Dodelson, & Widrow 1996; Bode et al. 2001), with typical dark matter particles of rest mass ~ 1 keV.

[1] Department of Physics and Center for Astrophysics and Space Sciences, University of California, San Diego, La Jolla, CA 92093-0319.
[2] Harvard-Smithsonian Center for Astrophysics, 60 Garden Street, Cambridge, MA 02138.

On the other hand, the lack of dwarf galaxies may be caused by feedback processes from supernovae and heating in small halos because of the initial formation of very massive stars in a zero-metallicity environment (Bullock, Kravtsov, & Weinberg 2001; Binney, Gerhard, & Silk 2001; Abel et al. 1998). However, it is not clear that these processes would be successful in disrupting dwarf galaxy formation. Nevertheless, there remain many mysteries regarding the earliest stars. Observations of abundances in ultra–metal-poor halo stars may be giving us some new insights into these issues. For example, Qian & Wasserburg (2001) have argued that an inferred increase in [Fe/H] with no concomitant increase in *r*-process abundances may signal the activity of very massive objects.

Another potential problem in CDM models is that the universal density profiles predicted in simulations of structure formation have a monotonic increase of density toward the center of halos. This could give a central "cusp," that is, a discontinuity in the derivative of the spatial density distribution that is a result of the initial singularity in velocity dispersion. The observational searches for a centrally peaked dark matter profile are as yet inconclusive (Swaters, Madore, & Trewhella 2000; van den Bosch et al. 2000). However, the measurement of the innermost rotation curve in dark matter–dominated galaxies may provide the dark matter profile of these halos.

One proposed solution to the central density problem is self-interacting dark matter (Spergel & Steinhardt 2000), which has strong interaction strength forces among dark matter particles and essentially no interactions between dark matter particles and ordinary matter. This kind of interaction would soften cores as a result of efficient energy exchange in halo centers.

In fact, however, Dalcanton & Hogan (2001) find that the core phase-space density distributions in dwarf galaxies and clusters may behave as simple power laws over 8 orders of magnitude in phase density. They argue that such density profiles could not arise from either a WDM or self-interacting dark matter scenario (see also Sellwood 2000).

The idea of using discrete UV photon sources to place limits on the radiative decay of active neutrino HDM was first proposed by Shipman & Cowsik (1981). The lack of UV photons from the rich cluster A665 was used by Melott et al. (1994) to constrain a decaying neutrino dark matter model proposed by Sciama (1990). Our approach to the detection of a radiative flux from cluster cores is similar: we explore the efficacy of X-ray observations in obtaining detections of or constraints on singlet neutrino, active neutrino, and gravitino dark matter candidates.

If observations fail to find the decay flux predicted for a specific dark matter candidate, then the decay constraints presented here can provide upper mass bounds on dark matter candidates. Together with existing structure-derived lower limits on the dark matter particle rest mass in these models, we can potentially exclude specific particle dark matter candidates.

For example, from observation of the power spectrum of the Lyα forest clouds at high redshift, it can be concluded that there is significant structure on small scales. This requires a small collisionless damping scale associated with a dark matter particle with a thermal energy spectrum, and in this limit the particle's rest mass must be greater than 750 eV for a standard warm dark matter particle that decoupled at high temperature (Narayanan et al. 2000). In addition, a paucity of power on small scales can delay the formation of structure at high redshifts and delay cosmological reionization. Such considerations corroborate the Lyα forest constraints and also favor a WDM particle to have a rest mass greater than 750 eV (Barkana, Haiman, & Ostriker 2001). The energy distribution for singlet neutrino relics is different from dark matter that has decoupled at high temperature and is generally "warmer." Colombi et al. (1996) find that the power spectrum for a sterile neutrino with rest mass m_s is the same for a standard WDM relic particle with rest mass m_X if $m_s \approx 2.6 m_X$. Therefore, current lower limits on singlet WDM particle rest mass favor singlet neutrinos with masses $m_s \gtrsim 2.0$ keV.

In § 2, we outline the radiative decay rates that can be probed in deep X-ray observations. Section 3 describes the singlet neutrino, active neutrino, and gravitino WDM candidates and their radiative decay modes. In § 4, we describe specific limits from field galaxy dark matter halos and those from clusters of galaxies. Section 5 presents current diffuse limits on singlet neutrino dark matter. In § 6, we present our conclusions.

2. DARK MATTER HALOS AS PARTICLE RESERVOIRS

An object such as a field galaxy or dwarf galaxy or a cluster of galaxies possessing a dark matter halo of mass $M_{\rm DM}$ will be composed of $N = M_{\rm DM}/m_X$ dark matter particles of rest mass m_X. If Γ_γ is the dark matter particle decay rate into photons of energy E_γ, then the total associated X-ray luminosity is

$$\mathscr{L} \approx \frac{E_\gamma}{m_X} M_{\rm DM} \Gamma_\gamma \, . \tag{1}$$

Here we have assumed that the halo is relatively nearby and that redshift effects on the luminosity are negligible.

For illustration let us take the case where $E_\gamma = m_X/2$ (here, and unless mentioned otherwise, we adopt units where $\hbar = c = 1$). The flux from an object is simply $F = \mathscr{L}/4\pi D_L^2$, where D_L is the luminosity distance to the object. With a reasonable integration time observation of a dark matter halo, a line of energy $E_\gamma = m_X/2$ can be detected at a flux above, for example, $F_{\rm det} = 10^{-13}$ ergs cm^{-2} s^{-1}. (We will show that this actually is the appropriate limit for *Chandra*.) This can place a limit on the radiative decay rate of the relic dark matter particle at

$$\Gamma_\gamma \lesssim (2.4 \times 10^{20} \text{ yr})^{-1} \left(\frac{F_{\rm det}}{10^{-13} \text{ ergs cm}^{-2} \text{ s}^{-1}} \right) \times \left(\frac{M_{\rm DM}^{\rm fov}}{10^{11}\, M_\odot} \right)^{-1} \left(\frac{D_L}{1 \text{ Mpc}} \right)^2 , \tag{2}$$

where $M_{\rm DM}^{\rm fov}$ is the total mass of dark matter within the observed field of view. As we show below, a decay rate limit of this magnitude can be significant in constraining singlet neutrino, active neutrino, and gravitino WDM candidate parameters.

3. WARM DARK MATTER PARTICLE CANDIDATES

3.1. *Singlet Neutrinos*

In general, the neutrino mass eigenstates ν_a ($a = 1, 2, \ldots$) are related by a unitary transformation to the flavor eigenstates ν_α ($\alpha = e, \mu, \tau, s, \ldots$):

$$\nu_a = \sum_\alpha U_{a\alpha} \nu_\alpha \, . \tag{3}$$

A singlet or "sterile" neutrino, ν_s, that has a very small mixing, $\sin^2 2\theta \approx 4|U_{1s}U_{2s}|^2 \ll 1$, with one or more doublet ("active") neutrinos, could be produced nonthermally via active neutrino scattering in the early universe. This was proposed as a WDM candidate by Dodelson & Widrow (1994). Singlet neutrino dark matter also could be produced by matter enhancement (a Mikheyev-Smirnov-Wolfenstein [MSW] resonance; Mikheyev & Smirnov 1985; Wolfenstein 1978) driven by a primordial net lepton number residing in the active neutrino seas (Shi & Fuller 1999). Interestingly, the singlet neutrino could be produced in the requisite numbers to be a WDM candidate in these scenarios even for extremely small vacuum mixing angles, $10^{-13} \lesssim \sin^2 2\theta \lesssim 10^{-7}$.

Supernova constraints on these scenarios were considered by G. M. Fuller.[3] Dolgov & Hansen (2000) did another calculation of the Dodelson & Widrow nonresonant scattering production scenario for WDM singlets and also discussed diffuse photon background and SN 1987A limits on these models.

Singlets with rest mass $m_s \gtrsim 1$ keV are produced during or prior to the quark-hadron transition. In this case, the effects of dilution, enhanced scattering rates, and the evolution of the thermal potential become important. Abazajian, Fuller, & Patel (2001; hereafter AFP) considered singlet WDM production in both the nonresonant Dodelson & Widrow and resonant Shi & Fuller modes and explicitly took account of these early universe thermodynamic effects. AFP also considered in detail constraints on these models arising from diffuse photon backgrounds, cosmic microwave background, ^{6}Li and ^{2}H, big bang nucleosynthesis, and supernova effects limits.

In these models the singlet neutrino is produced in the early universe through nonequilibrium scattering processes involving active neutrinos and other weakly interacting particles. (Singlet neutrinos could be produced via coherent MSW resonance in one limit of matter-enhancement scenarios.) In the matter-enhanced, resonant singlet neutrino production scenarios, the relic density and energy spectrum of the singlet neutrinos can depend on the initial neutrino lepton number residing in the active neutrino seas:

$$L_{\nu_\alpha} \equiv \frac{n_{\nu_\alpha} - n_{\bar{\nu}_\alpha}}{n_\gamma}, \tag{4}$$

where $n_{\nu_\alpha}(n_{\bar{\nu}_\alpha})$ is the neutrino (antineutrino) number density and $n_\gamma = 2\zeta(3)T^3/\pi^2 \approx 0.243T^3$ is the photon number density. In the case of small initial neutrino lepton number ("small" here means the same order of magnitude or smaller than the baryon-to-photon ratio $\eta \sim 10^{-10}$), $L_{\nu_\alpha} \approx 0$, the production occurs at larger mixing angles than in the nonstandard yet plausible case of a large lepton number, $0.001 \lesssim L_{\nu_\alpha} \lesssim 1$. For large lepton numbers, production is resonantly enhanced at low energies, and the energy spectrum of the singlet neutrinos can be "cooler" (that is, possess a smaller collisionless damping scale) than for the case of a thermal energy spectrum (Shi & Fuller 1999).

For the $L_{\nu_\alpha} \approx 0$ case, the fraction of the closure density in singlet neutrinos that is produced in the early universe was found by AFP to be approximately

$$\Omega_{\nu_s} h^2 \approx 0.3\left(\frac{\sin^2 2\theta}{10^{-10}}\right)\left(\frac{m_s}{100\ \mathrm{keV}}\right)^2. \tag{5}$$

Here θ is the vacuum mixing angle defined by an *effective* two-by-two unitary transformation between active ν_α species and a singlet species ν_s:

$$|\nu_\alpha\rangle = \cos\theta|\nu_1\rangle + \sin\theta|\nu_2\rangle,$$
$$|\nu_s\rangle = -\sin\theta|\nu_1\rangle + \cos\theta|\nu_2\rangle, \tag{6}$$

where $|\nu_1\rangle$ and $|\nu_2\rangle$ represent neutrino energy (mass) eigenstates corresponding to vacuum mass eigenvalues m_1 and m_2, respectively. Here we define $h = H_0/(100\ \mathrm{km\ s^{-1}\ Mpc^{-1}})$, where H_0 is the Hubble parameter at the current epoch. It should be kept in mind that future calculations with more sophisticated treatments of the singlet neutrino production physics and the early universe environment may sharpen up, shift, or possibly extend the mass/mixing parameter range that gives interesting relic dark matter contributions.

For nonnegligible lepton numbers, the singlet closure fraction produced depends on the precise value of L_{ν_α} as well as the mixing angle and mass of the singlet neutrino. In general, the matter-enhanced ($L_{\nu_\alpha} \neq 0$) singlet neutrino production modes can produce the same closure fraction as the $L_{\nu_\alpha} \approx 0$ models but do so with orders of magnitude smaller vacuum mixing angles (Shi & Fuller 1999; AFP). As a result, it is in general harder to constrain the $L_{\nu_\alpha} \neq 0$ singlet neutrino production mode scenarios.

Significant constraints can be made on massive neutrinos via the effects of their decay (Dicus, Kolb, & Teplitz 1978). The primary decay channel of massive singlet neutrinos is into three light active neutrinos and is shown in Figure 1. The decay rate corresponding to this process is (Barger, Phillips, & Sarkar 1995; Boehm & Vogel 1987)

$$\Gamma_{3\nu} \approx \sin^2 2\theta G_F^2\left(\frac{m_s^5}{768\pi^3}\right)$$
$$\approx 8.7 \times 10^{-31}\ \mathrm{s^{-1}}\left(\frac{\sin^2 2\theta}{10^{-10}}\right)\left(\frac{m_s}{1\ \mathrm{keV}}\right)^5, \tag{7}$$

where $G_F \approx 1.166 \times 10^{-11}\ \mathrm{MeV^{-2}}$ is the Fermi constant. This process needs to be considered when comparing number densities of singlets produced at a very early time with those today, for example, in the calculation of the diffuse extragalactic background radiation (see § 5).

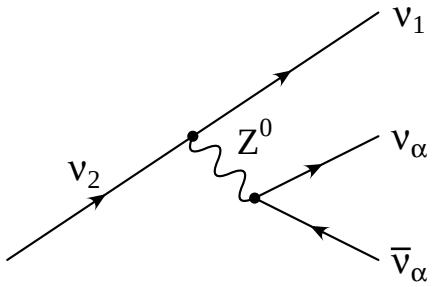

FIG. 1.—Principal decay mode for massive singlet neutrinos with mass less than twice the electron mass. There are three light active neutrinos in the final state. (Here, $\alpha = e$, μ, and τ.)

[3] Fuller, G. M. 2000, Neutrino Astrophysics and Cosmology (lectures at the XXVIII SLAC Summer Institute on Particle Physics: Neutrinos from the Lab, the Sun, and the Cosmos). Available at http://www.slac.stanford.edu/gen/meeting/ssi/2000/fuller.html.

The principal radiative decay modes of singlet neutrinos are shown in Figure 2. Majorana neutrinos have contributions from conjugate processes. For the Majorana neutrino case, the decay rate for $m_2 \gg m_1$ is (Pal & Wolfenstein 1982)

$$\Gamma_\gamma = \frac{\alpha G_F^2}{64\pi^4} m_2^5 \left[\sum_\beta U_{1\beta} U_{2\beta} F(r_\beta) \right]^2 , \quad (8)$$

where $\alpha \approx 1/137$ is the fine-structure constant. Here, $r_\beta = (m_\beta/M_W)^2$ is the square of the ratio of the β flavor charged lepton mass and the $W^\pm$ boson mass, and

$$F(r_\beta) \approx -\tfrac{3}{2} + \tfrac{3}{4} r_\beta . \quad (9)$$

The sum in equation (8) is over the charged lepton flavors. For decay of a doublet neutrino into another flavor doublet, the sum in equation (8) vanishes for the first term in equation (9) on account of the unitarity property associated with the transformation matrix elements in equation (3). The second term in equation (9) causes the sum not to vanish, but the resulting term is obviously very small because it involves the fourth power of the ratio of charged lepton to $W^\pm$ masses. This is the so-called Glashow-Iliopoulos-Maiani (GIM) suppression (or cancellation).

For a singlet decay, the sum over the charged lepton flavors in equation (9) does not cancel the leading contribution in equation (9) because there is no charged lepton associated with the singlet state. The decay rate is consequently greatly enhanced over the GIM-suppressed doublet decay case. The rate of singlet neutrino radiative decay is

$$\Gamma_\gamma(m_s, \sin^2 2\theta) \approx 6.8 \times 10^{-33} \text{ s}^{-1} \left(\frac{\sin^2 2\theta}{10^{-10}} \right) \left(\frac{m_s}{1 \text{ keV}} \right)^5 , \quad (10)$$

where we have identified $m_s \approx m_2$, since the mixing is presumed to be small.

The singlet neutrino can also decay via two-photon emission, $\nu_2 \rightarrow \nu_1 + \gamma + \gamma$. However, this decay has a leading contribution scaling with the inverse square of the charged lepton mass (Nieves 1983) and therefore is strongly suppressed. Since the two-photon decay rate scales as m_s^9, it will dominate over the single-photon mode for masses $m_s \gtrsim 10$ MeV. However, singlet neutrino masses over 10 MeV are excluded by other considerations (AFP).

In the case of the single-photon channel, the decay of a nonrelativistic singlet neutrino into two (nearly) massless particles produces a line at energy $E_\gamma = m_s/2$ with a width given by the velocity dispersion of the dark matter. For example, clusters of galaxies typically have a virial velocity dispersion of ~ 300 km s^{-1}. Therefore, the emitted line is very narrow, $\Delta E \sim 10^{-3} E_\gamma$. The observed width of the line will be given by the energy resolution of the detector in this case. For example, the energy resolution of *Chandra*'s Advanced CCD Imaging Spectrometer (ACIS) is $\Delta E \approx 200$ eV, while the Constellation X project hopes to achieve a resolution of $\Delta E \approx 2$ eV.

The luminosity from a general singlet neutrino dark matter halo is (from eq. [1])

$$\mathcal{L} \approx 6.1 \times 10^{32} \text{ ergs s}^{-1} \left(\frac{M_{DM}}{10^{11} M_\odot} \right) \left(\frac{\sin^2 2\theta}{10^{-10}} \right) \left(\frac{m_s}{1 \text{ keV}} \right)^5 . \quad (11)$$

This implies that the radiative decay flux from singlet neutrinos in the halo is

$$F \approx 5.1 \times 10^{-18} \text{ ergs cm}^{-2} \text{ s}^{-1} \left(\frac{D_L}{1 \text{ Mpc}} \right)^{-2} \times \left(\frac{M_{DM}}{10^{11} M_\odot} \right) \left(\frac{\sin^2 2\theta}{10^{-10}} \right) \left(\frac{m_s}{1 \text{ keV}} \right)^5 . \quad (12)$$

Therefore, for a general singlet neutrino candidate with rest mass m_s and vacuum mixing angle $\sin^2 2\theta$, the mass limit—assuming no detection of a line at a flux limit level of F_{det}—is

$$m_s \lesssim 4.6 \text{ keV} \left(\frac{D_L}{1 \text{ Mpc}} \right)^{2/5} \left(\frac{F_{det}}{10^{-13} \text{ ergs cm}^{-2} \text{ s}^{-1}} \right)^{1/5} \times \left(\frac{M_{DM}}{10^{11} M_\odot} \right)^{-1/5} \left(\frac{\sin^2 2\theta}{10^{-10}} \right)^{-1/5} . \quad (13)$$

Using equation (5), the dependence on mixing angle can be eliminated, and with equation (1), we have for the $L_{\nu_\alpha} \approx 0$ case that the flux due to singlet neutrino decay is

$$F \approx 5.1 \times 10^{-14} \text{ ergs cm}^{-2} \text{ s}^{-1} \left(\frac{D_L}{1 \text{ Mpc}} \right)^{-2} \times \left(\frac{M_{DM}}{10^{11} M_\odot} \right) \left(\frac{\Omega_{\nu_s} h^2}{0.3} \right) \left(\frac{m_s}{1 \text{ keV}} \right)^3 . \quad (14)$$

For the $L_{\nu_\alpha} \approx 0$ production case, the corresponding singlet mass limit from a null detection of a line at $E_\gamma = m_s/2$ at flux limit F_{det} is

$$m_s \lesssim 1.25 \text{ keV} \left(\frac{D_L}{1 \text{ Mpc}} \right)^{2/3} \left(\frac{F_{det}}{10^{-13} \text{ ergs cm}^{-2} \text{ s}^{-1}} \right)^{1/3} \times \left(\frac{M_{DM}}{10^{11} M_\odot} \right)^{-1/3} \left(\frac{\Omega_{\nu_s} h^2}{0.3} \right)^{-1/3} . \quad (15)$$

It should be noted that the decay limits presented here derive from a specific type of mass-generation mechanism

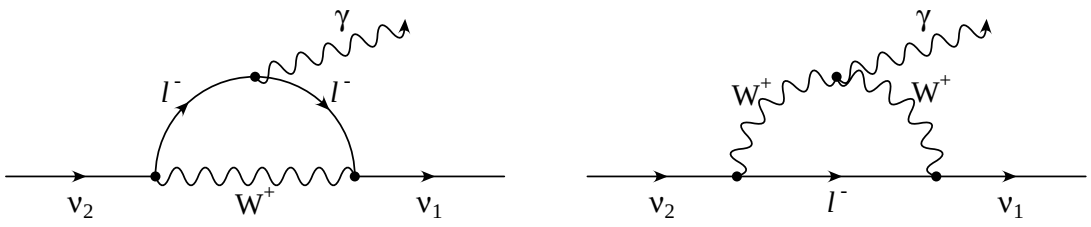

FIG. 2.—Principal radiative decay modes for massive singlet neutrinos

for the singlet neutrino: those arising from the simplest case of Majorana or Dirac-type mass terms. More complicated neutrino mass models would have different mass terms, radiative decay widths, and possibly other couplings, and bounds on these models would require individual analysis.

3.2. *Active Neutrinos*

The direct experimental upper limits on the ν_μ and ν_τ masses are only 190 keV and 18.2 MeV, respectively (Groom et al. 2000). Although the observationally inferred age of the universe precludes the possibility of fully thermalized active neutrinos being the WDM or CDM (Gerstein & Zeldovich 1966; Cowsik & McClelland 1972), the active neutrinos may not be fully thermalized in the early universe if the postinflation reheating temperature is low (Kawasaki, Kohri, & Sugiyama 2000; Giudice, Kolb, & Riotto 2001a). In this case, the ν_μ and/or ν_τ can be legitimate WDM candidates (Giudice et al. 2001b).

The radiative decay rate of massive active neutrinos into a single photon in a three-generation neutrino model is suppressed by the GIM mechanism and is slower than the singlet neutrino decay rate by a factor $(m_\alpha/M_W)^4 \sim 10^{-21}$, and therefore negligible. The two-photon decay mode $\nu_2 \rightarrow \nu_1 + \gamma + \gamma$ for massive active neutrino decay has a GIM suppression factor of $\sim(m_a/m_\alpha)^4$, where m_a is the relevant vacuum neutrino mass eigenvalue and m_α is the mass of the charged lepton of flavor α (Nieves 1983). This rate can therefore dominate the single-photon mode only for $m_a \gtrsim$ 200 keV, which is outside of the range of interest for active neutrino WDM. Therefore, active neutrino WDM in a three-generation neutrino model is relatively stable and robust against decay constraints.

In order to accommodate solar and atmospheric neutrino oscillation solutions to experimental data, a light singlet neutrino with mass $m_s \ll m_{\nu_{\mu,\tau}}$ must be a feature of any neutrino mass/mixing scheme that can provide for an active ν_μ/ν_τ WDM candidate. If there is a light singlet, then the decay from the mass eigenstates most closely associated with the ν_μ/ν_τ doublet into a mass state more closely associated with the lighter singlet is not GIM suppressed. This process can lead to a rapid radiative decay of the active WDM candidate. However, the mixing between the two mass eigenstates can be tuned to be arbitrarily small, since it is not phenomenologically required to be nonzero. If a spectral feature in the X-ray is observed, however, it may indicate a nonnegligible mixing between a massive active neutrino and a lighter singlet neutrino.

3.3. *Gravitinos*

Another WDM candidate is the gravitino, $\tilde{G}$, the spin $\frac{1}{2}$ supersymmetric partner to the graviton (Kawasaki, Sugiyama, & Yanagida 1997). In the minimal supersymmetric standard model, the assumption of R-parity conservation is made, originally motivated by the need to explain the slow proton decay rate. The gravitino can be the lightest supersymmetric particle (LSP) and, with R-parity conservation, it is stable. However, there has been considerable interest in R-parity violation in supersymmetric models as a mechanism for neutrino mass generation (Hall & Suzuki 1984), motivated by the considerable evidence for neutrino mass (for a review, see Caldwell 1998). The gravitino may also be the LSP and the dark matter (Takayama & Yamaguchi 2000) in R-parity–violating models with gauge mediation (Dine et al. 1996) or with a low gravitational scale (or effective Planck scale $M_{\rm Pl}$), which comes about through large extra dimensions (Arkani-Hamed, Dimopoulos, & Dvali 1998).

The gravitino LSP decays with a long lifetime in these models since its decay is suppressed by $M_{\rm Pl}^2$. In one specific example considered by Takayama & Yamaguchi (2000), the R-parity violation is bilinear, with the lightest neutralino being bino-dominant. In this case, the dominant decay mode of the gravitino is $\tilde{G} \rightarrow \gamma\nu$ through a coupling of the gravitino with the photon and its superpartner, the photino, which has a neutrino component. The lifetime of the gravitino is approximately

$$\Gamma_\gamma(\tilde{G} \rightarrow \gamma\nu) \approx \frac{1}{4} |U_{\gamma\nu}|^2 \frac{m_{3/2}^3}{M_{\rm Pl}^2}, \tag{16}$$

where $U_{\gamma\nu}$ represents the neutrino component of the photino and $m_{3/2}$ is the gravitino mass.

In the models accommodating neutrino masses associated with the atmospheric neutrino problem, $U_{\gamma\nu}$ has a characteristic value $|U_{\gamma\nu}|^2 \approx 7 \times 10^{-13}$. The decay rate of the gravitino into photons is then

$$\Gamma_\gamma(\tilde{G} \rightarrow \gamma\nu) \approx (2.6 \times 10^{19}\ \text{yr})^{-1} \left(\frac{m_{3/2}}{1\ \text{GeV}}\right)^3 \times \left(\frac{|U_{\gamma\nu}|^2}{7 \times 10^{-13}}\right) \left(\frac{M_{\rm Pl}}{M_{\rm Pl}^0}\right)^{-2}, \tag{17}$$

where $M_{\rm Pl}^0 \approx 1.22 \times 10^{19}$ GeV is the conventional Planck scale. The decay would produce a photon line at an energy of $E_\gamma \approx m_{3/2}/2$. For a $\sim$1 keV mass gravitino, the decay rate is far below the detectable limit given by equation (2). However, as mentioned previously, the gravitino is the LSP in some supersymmetric models with large extra dimensions. These scenarios generically reduce the effective Planck scale by up to 14 orders of magnitude. From equation (17), if the effective Planck scale is reduced by "only" 7 orders of magnitude, the rate becomes detectable. Ultimately, the lack or presence of a photon emission line may constrain supersymmetric dark matter models with large extra dimensions.

4. OBSERVING DARK MATTER HALOS

Astronomical objects with strong evidence for dark matter concentrations can serve as source reservoirs for WDM particles. The specific amount of dark matter in the observed region can be inferred from models of the spatial distribution of the dark matter. The theoretical basis for the dark matter distribution is based on either local or cosmological physics.

Local models include truncated isothermal sphere configurations, which describe galactic dark matter halos as perfect gases in equilibrium. The isothermal sphere model reproduces well the observed flat rotation curves of spiral galaxies. In another local-type model, the dark matter in X-ray clusters of galaxies is assumed to be the dominant source of the gravitational potential binding the hot X-ray–emitting intracluster medium in hydrostatic equilibrium in the β-model.

In CDM models, both galaxy and galaxy cluster halos can be the result of hierarchical clustering and so can possess a unified profile. However, CDM models and their corresponding unified profiles may be too centrally concentrated to describe dwarf galaxy rotation curves (Navarro,

Frenk, & White 1995, 1996). The general dark matter density profile with radius $\rho(r)$ for hierarchical clustering is dubbed the Navarro-Frenk-White (NFW) profile:

$$\rho(r) \propto \left(\frac{r}{r_s}\right)^{-1}\left(1+\frac{r}{r_s}\right)^{-2}, \quad (18)$$

where r_s is the scale radius.

Given any dark matter distribution for an object, the photon flux resulting from particle decay or interaction is simply proportional to the mass within the field of view. This can be approximated as the mass within the projected radius at the distance of the object. However, the dark matter in the field of view contains not only the extended halo out to the projected radius but also the material in front of and behind this sphere. To determine the mass within the rectangular prism cut out of the extended halo of the object, we have performed a Monte Carlo integration of the region's mass density, sampling according to an assumed density profile, e.g., NFW.

4.1. *Instrumental Background*

For low surface brightness dark matter systems, the primary limit to dark matter flux detection is instrumental background. In particular, ACIS aboard *Chandra* has a background of 2×10^{-2} counts s^{-1} in a $\sim$200 eV energy bin of the imaging array.

As a rough approximation, we can estimate the flux onto ACIS from dark matter decay requisite to produce a 4 σ detection. For a line with flux $F_{-14} \equiv F/(10^{-14}$ ergs cm^{-2} s$^{-1})$, the count rate is $C_L \approx 3 \times 10^{-4} F_{-14}$ counts s^{-1}. For an observation of integration time $t_5 \equiv t/(10^5$ s), the background is $B \approx 2 \times 10^3 t_5$ counts. The count level required to overcome the background at 4 σ is

$$C_L \approx \frac{4\sqrt{B}}{t}. \quad (19)$$

Therefore, the detectable flux is

$$F_{-14}^{\rm det} \approx 6 t_5^{-1/2}. \quad (20)$$

For low surface brightness sources, an observation with an integration time of 36,000 s ($t_5 = 0.36$) can detect a flux $\approx 10^{-13}$ ergs cm^{-2} s^{-1} ($F_{-14}^{\rm det} = 10$). One must modify the estimated detectable WDM flux whenever the baryon-associated material (e.g., electrons, protons, iron, etc.) in these halos provides an ambient X-ray flux in excess of 3×10^{-11} ergs cm^{-2} s^{-1}. In such circumstances the minimum detectable WDM flux in a $\sim$200 eV energy bin, corresponding to the ACIS energy resolution, is

$$F_{-14}^{\rm det} \approx 6\left(\frac{F_{\rm source}}{3 \times 10^{-11}}\right)^{1/2} t_5^{-1/2} \text{ ergs cm}^{-2} \text{ s}^{-1}. \quad (21)$$

In Figure 3 we show contours of WDM X-ray photon decay flux in lines at photon energies $E_\gamma = m_s/2$ as a function of the dark matter mass in the field of view modulo its luminosity distance (see eq. [14]) for a WDM singlet neutrino model with zero initial lepton number, $L_{\nu_\alpha} \approx 0$. This figure provides a shaded region indicating detectability with ACIS on *Chandra* for a 36 ks observation.

4.2. *Clusters of Galaxies*

Clusters of galaxies are massive objects ($\sim 10^{15} M_\odot$), and there is strong evidence that most of this mass is carried by dark matter. Mass estimates are derived from a spherical hydrostatic equilibrium model that assumes that the gas in the intracluster medium is solely supported by thermal pressure. The enclosed mass at a radius r is given by

$$M(<r) = -\frac{kT_{\rm X}(r)}{G\mu m_p} r\left[\frac{d\log \rho_g(r)}{d\log r} + \frac{d\log T_{\rm X}(r)}{d\log r}\right], \quad (22)$$

where $G = (M_{\rm Pl}^0)^{-2}$, μm_p is the average molecular weight of the gas (m_p is the proton mass), k is Boltzmann's constant, $\rho_g(r)$ is the gas density profile, and $T_{\rm X}(r)$ is the temperature profile. Using this equilibrium model, an approximate isothermal fit to the mass profile can be made. This is the so-called isothermal β-model. The enclosed mass for the isothermal β-model is

$$M(<r) \approx 1.13 \times 10^{14} M_\odot \left(\frac{T_{\rm X}}{\rm keV}\right)\left(\frac{r}{\rm Mpc}\right)\frac{(r/r_c)^2}{1+(r/r_c)^2}, \quad (23)$$

where r_c is the core radius (Cavaliere & Fusco-Femiano 1978). (Note that r_c and r_s are related but not identical.)

With contemporary X-ray telescopes (*ASCA*, *XMM-Newton*, and *Chandra*) able to provide spatially resolved temperature profiles, the hydrostatic equilibrium β-model in principle can yield accurate mass estimates. However, as yet, detailed analyses along these lines to provide $T_{\rm X}(r)$ are still being done. Therefore, we employ the isothermal β-model with average temperature values. These are available for the 24 clusters that we consider.

In this work we use the average temperatures of rich clusters from the Horner, Mushotzky, & Scharf (1999) database. Redshifts or distances are taken from the SIMBAD database.[4] The physical properties of the clusters that we consider are given in Table 1.

We can approximate the reservoir of dark matter mass and observable decay flux for singlet neutrino dark matter seen by ACIS aboard the *Chandra* observatory using the relation between the projected radius of the field of view, $R_{\rm fov}$, and the angular field of view of ACIS, $\theta_{\rm fov} \approx 5 \times 10^{-3}$ rad: $D_L = 2R_{\rm fov}/\theta_{\rm fov} \approx 4 \times 10^2 R_{\rm fov}$. With equation (14), for the $L_{\nu_\alpha} \approx 0$ case, the expected X-ray flux is then

$$F \approx 3 \times 10^{-19} \text{ ergs cm}^{-2} \text{ s}^{-1}\left(\frac{m_s}{\rm keV}\right)^3\left(\frac{\Omega_{\nu_s} h^2}{0.3}\right) \times \left(\frac{M_{\rm DM}}{10^{11} M_\odot}\right)\left(\frac{R_{\rm fov}}{1 \text{ Mpc}}\right)^{-2}. \quad (24)$$

The core radius falls within the field of view of *Chandra* for all clusters that we consider except for the Coma Cluster. Since the mass increases approximately with the radius outside of the core, we can approximate $M_{\rm fov} \sim M_{\rm core} R_{\rm fov}/r_c$. Therefore, the expected X-ray flux from the cluster in the $L_{\nu_\alpha} \approx 0$ model is

$$\begin{aligned} F &\approx 3 \times 10^{-19} \text{ ergs cm}^{-2} \text{ s}^{-1}\left(\frac{m_s}{\rm keV}\right)^3\left(\frac{M_{\rm core}}{10^{11} M_\odot}\right) \times \left(\frac{r_c}{1 \text{ Mpc}}\right)^{-1}\left(\frac{R_{\rm fov}}{1 \text{ Mpc}}\right)^{-1} \\ &\approx 1.2 \times 10^{-16} \text{ ergs cm}^{-2} \text{ s}^{-1}\left(\frac{m_s}{\rm keV}\right)^3 \times \left(\frac{M_{\rm core}}{10^{11} M_\odot}\right)\left(\frac{D_L}{1 \text{ Mpc}}\right)^{-1}\left(\frac{R_{\rm fov}}{1 \text{ Mpc}}\right)^{-1}. \end{aligned} \quad (25)$$

[4] Available at http://simbad.u-strasbg.fr.

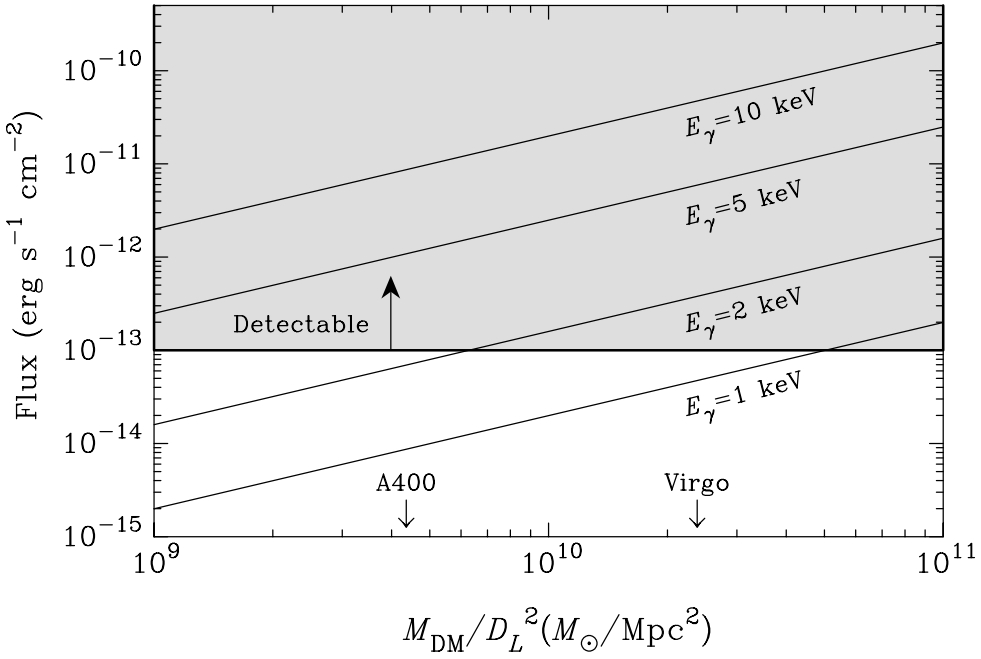

FIG. 3.—Singlet neutrino decay X-ray flux produced by an object with a mass M_{DM} at distance D_L. Shown are contours that correspond to spectral lines with energy E_γ produced by singlet neutrinos of mass $m_s = 2E_\gamma$. The shaded region indicates detectability with ACIS on *Chandra* for a 36 ks observation.

In order to more accurately determine the dark matter mass and luminosity in decay photons, we estimate the dark matter mass within the rectangular prism cut out of the spherical isothermal β-model density distribution in the dark matter halo. The prism has the dimensions of $2R_{fov} \times 2R_{fov} \times 2R_{vir}$, where R_{fov} is half the projected size of the aperture, $R_{fov} \approx \theta_{fov} D_L/2$, and where R_{vir} is the cluster's virial radius. We use a Monte Carlo integration to find the

TABLE 1

CLUSTERS OF GALAXIES

Name	$M_{vir}(M_X)$[a] ($\times 10^{14}\ h^{-1}\ M_\odot$)	r_c[a] (h^{-1} Mpc)	M_{core}[b] ($\times 10^{14}\ M_\odot$)	M_{DM}^{fov}[c] ($\times 10^{14}\ M_\odot$)	Γ_γ Limit[d] (yr^{-1})	$m_s(L_{\nu_\alpha} \approx 0)$ Limit[e] (keV)
2A0335+096.....	(1.10)	0.023	0.036	1.04	$(1.1 \times 10^{19})^{-1}$	4.5
A0085.....	9.88	0.086	0.313	3.53	$(1.6 \times 10^{19})^{-1}$	3.9
A0119.....	2.50	0.231	0.312	2.23	$(1.4 \times 10^{19})^{-1}$	4.1
A0262.....	1.32	0.032	0.029	0.33	$(1.6 \times 10^{19})^{-1}$	3.9
A0400.....	2.49	0.051	0.076	0.47	$(1.0 \times 10^{19})^{-1}$	4.5
A0426.....	9.08	0.020	0.063	1.08	$(4.3 \times 10^{19})^{-1}$	2.8
A0496.....	3.20	0.035	0.058	1.40	$(1.6 \times 10^{19})^{-1}$	3.9
A0539.....	2.01	0.082	0.094	1.00	$(1.6 \times 10^{19})^{-1}$	4.0
A1060.....	1.90	0.040	0.045	0.38	$(3.7 \times 10^{19})^{-1}$	2.9
A1656.....	4.97	0.208	0.245	1.98	$(4.7 \times 10^{19})^{-1}$	2.7
A1795.....	5.86	0.068	0.171	4.20	$(1.3 \times 10^{19})^{-1}$	4.2
A2063.....	3.04	0.067	0.110	1.43	$(1.4 \times 10^{19})^{-1}$	4.1
A2199.....	5.71	0.040	0.102	1.42	$(2.0 \times 10^{19})^{-1}$	3.6
A2256.....	23.12	0.228	1.40	5.26	$(1.8 \times 10^{19})^{-1}$	3.8
A2319.....	39.54	0.135	1.24	4.87	$(1.9 \times 10^{19})^{-1}$	3.7
A2634.....	4.31	0.123	0.273	0.98	$(1.3 \times 10^{19})^{-1}$	4.2
A3526.....	(0.80)	0.038	0.043	0.37	$(3.9 \times 10^{19})^{-1}$	2.9
A3558.....	11.54	0.075	0.318	2.22	$(1.2 \times 10^{19})^{-1}$	4.3
A3571.....	8.17	0.086	0.241	2.95	$(2.3 \times 10^{19})^{-1}$	3.5
A4059.....	(1.50)	0.075	0.164	1.73	$(1.0 \times 10^{19})^{-1}$	4.6
AWM 7	5.77	0.062	0.148	0.65	$(2.8 \times 10^{19})^{-1}$	3.3
MKW 3S.....	(2.00)	0.047	0.067	1.83	$(1.2 \times 10^{19})^{-1}$	4.3
MKW 4	1.15	0.009	0.0070	0.30	$(9.7 \times 10^{18})^{-1}$	4.6
Virgo	2.04	0.007	0.0081	0.10	$(5.6 \times 10^{19})^{-1}$	2.6

[a] The values of M_{vir} and r_c are from Horner et al. 1999. For clusters whose M_{vir} is not well known, we used the mass determined by the X-ray profile, M_X (shown in parentheses).

[b] The mass within the core radius M_{core}.

[c] The mass within the field of view M_{DM}^{fov} (density integrated over the rectangular prism in the field of view).

[d] The potential limit on the radiative decay rate Γ_γ of dark matter from the object with a 36 ks observation.

[e] The corresponding constraint on the singlet neutrino mass, m_s, in the $L_{\nu_\alpha} \approx 0$ case (eq. [15]).

dark matter mass within this field of view, which can be significantly larger than the mass strictly within the spherical volume defined by the core radius.

We can use equation (15) to provide a rough limit on the mass m_s of a singlet neutrino candidate assumed to comprise the dark matter halo. The limits on m_s for various clusters are given in Table 1. The best limit, $m_s \lesssim 2.6$ keV (for the $L_{\nu_\alpha} \approx 0$ case), is provided by the Virgo Cluster.

In Figure 4 we give contours in singlet mass m_s and vacuum mixing angle space of singlet neutrino closure fraction $\Omega_s \approx 0.3$ (for $h = 0.7$) for three values of primordial lepton number ($L \equiv L_{\nu_\alpha}$): $L \approx 0$, $L \approx 0.01$, and $L \approx 0.1$. The nonzero lepton number contours are very rough fits to the results of AFP. (Note that lepton number L here is denoted as $\mathscr{L}$ in AFP.) Superimposed on this figure are shaded regions indicating potential detectability or exclusion of singlet neutrino WDM from *Chandra* observations of the Virgo Cluster for a 36 ks observation (*dark shade bounded by the solid line*) and a 100 ks observation (*bounded by the dashed line*). The *Chandra* observations of the Virgo Cluster can come close to eliminating all of the $L \approx 0$, nonresonant singlet production mode case. In the next section, we will argue that the Constellation X project can give even broader constraints in this figure.

To study the possible observational signature of a singlet neutrino halo in the Virgo Cluster, we generate spectra of the gas in Virgo as seen with ACIS with WEBSPEC (XSPEC). We use the MEKAL model for the X-ray flux for the gas at a temperature of 2.54 keV (Horner et al. 1999) with a thermal X-ray flux from the central region of 1.5×10^{-12} ergs cm^{-2} s^{-1} in the 2–10 keV band (Böhringer et al. 2001). We adopt a distance to the Virgo cluster of 20.7 Mpc measured from 21 cm line widths by Federspiel, Tammann, & Sandage (1998).

In Figure 5, we show the binned spectrum for two cases. We include the decay fluxes (see eq. [14]) from a singlet neutrino halo composed of 4 and 5 keV singlet neutrinos producing decay photons of energy 2 and 2.5 keV, respectively, for a 50 ks observation on *Chandra*'s ACIS. In addition, we include the theoretical MEKAL model gas emission spectrum. The residuals from this standard gas emission prediction are given at the bottom of the figure. The width of the lines is nearly entirely due to instrumental broadening.

From this unsophisticated example, it is obvious that a line feature produced by a 5 keV singlet neutrino would be readily detectable, while the detection/elimination of the decay line for a 4 keV singlet would require a statistical analysis. With the lack of such a strong line anomaly in the observation of M87 in the core of the Virgo Cluster with *XMM-Newton* by Böhringer et al. (2001), we can conclude that the dark matter in the Virgo Cluster is not composed of singlet neutrinos with masses $m_s \gtrsim 5$ keV created in the early universe with $L_{\nu_\alpha} \approx 0$. The potential constraints on general L_{ν_α} scenarios from statistical spectral analyses are shown in Figure 4.

4.3. *Field Spiral Galaxies*

Field galaxies can provide low gas X-ray emission sources for dark matter, but these objects do not represent as concentrated a dark matter source as do clusters of galaxies. A detailed observation of the structure and rotation of NGC 4123 has allowed a fit to disk and halo models that places a lower limit on the profile of the dark matter halo

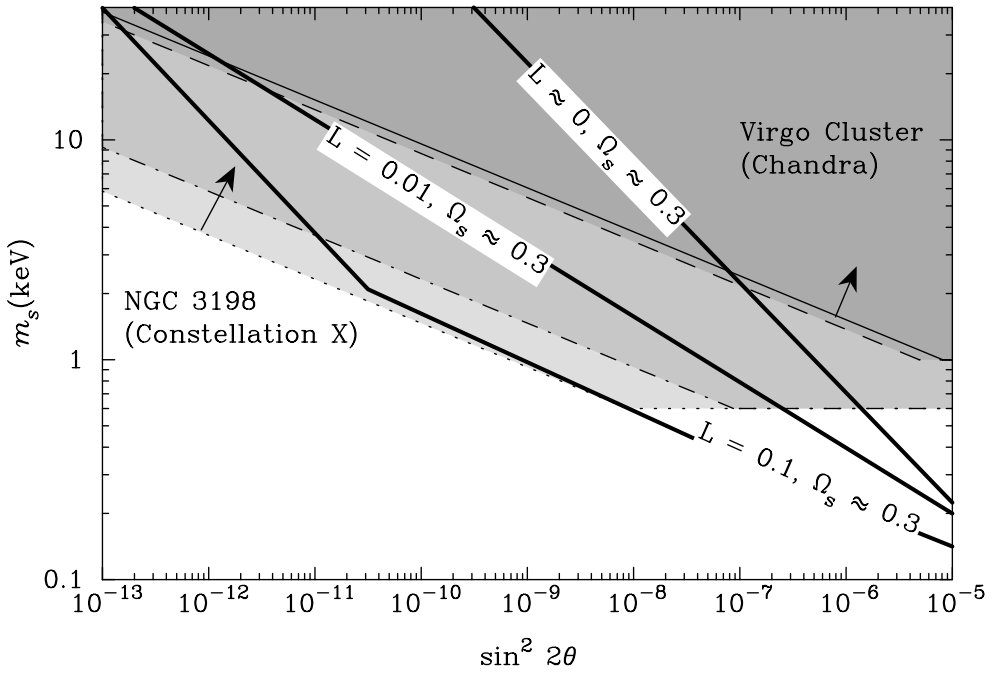

FIG. 4.—Shown are approximate contours for $\Omega_s \approx 0.3$ ($h = 0.7$) for singlet neutrino WDM models with different initial lepton number, L. Potential detection/exclusion of the models can be made in the darkest gray region with a limiting line flux of 10^{-13} ergs cm^{-2} s^{-1} from the Virgo Cluster observed with *Chandra*'s ACIS (from a 36 ks observation). The dashed line is the limit for a 100 ks observation with *Chandra*, also for Virgo. The medium-gray region bounded by the dashed-dotted line indicates the detection/exclusion range for Constellation X observation of field spiral galaxy NGC 3198 for a 1000 ks observation, and the light-gray region indicates the possibility of detection/exclusion for an ambitious 10 Ms observation (presumably obtained in several observations over a few years).

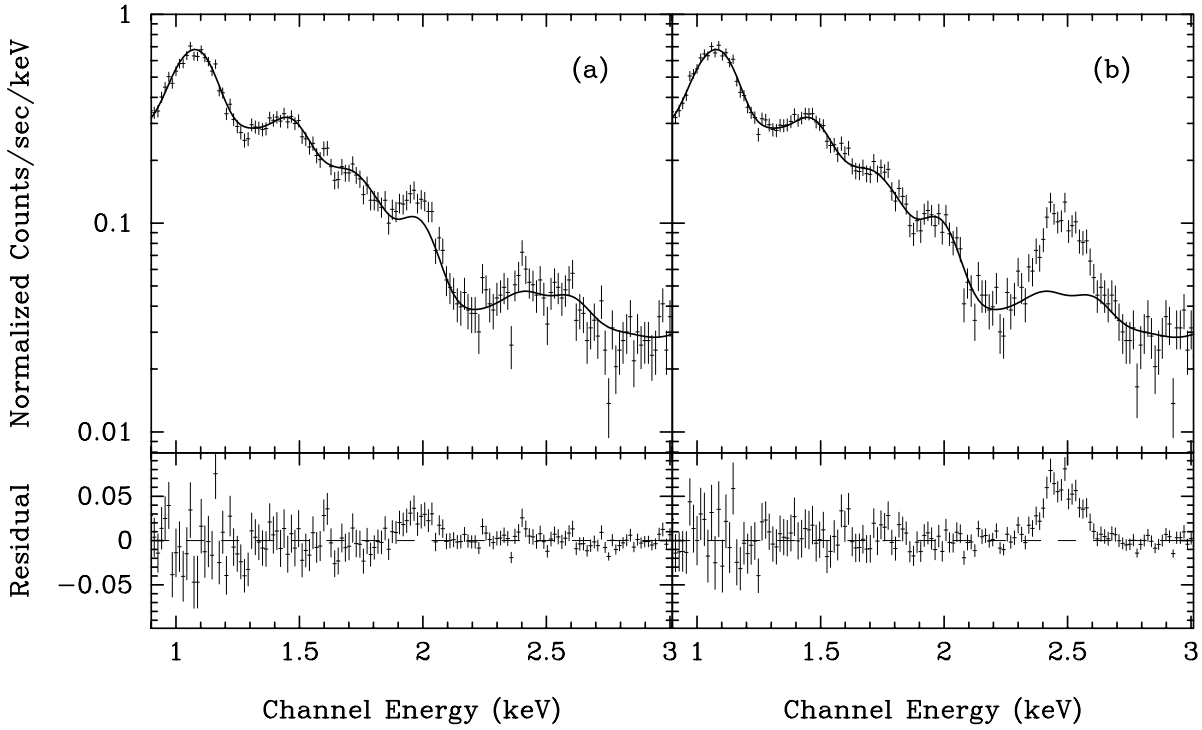

FIG. 5.—Synthesized spectrum viewed by *Chandra*'s ACIS modeling the central region of the Virgo Cluster, for two different cases of singlet neutrino mass, showing a strong mass dependence of the flux in a line at (*a*) a 4 keV singlet neutrino halo (producing a 2 keV line) and (*b*) a 5 keV singlet neutrino halo (producing a 2.5 keV line). Integration time is assumed to be 50 ks, with a $T_X = 2.54$ keV thermal flux (1.5×10^{-12} ergs cm^{-2} s^{-1}) from the gas in Virgo generated with the MEKAL model, which is shown as the solid line. Residuals from the gas emission model alone are shown at the bottom. The width of the line is nearly entirely due to instrumental energy resolution.

(Weiner et al. 2001). Using a maximal disk model to fit the observed rotation curve, they find that a dark halo remains required. We use an NFW-type profile halo fitted by Weiner et al. (2001) and find the resulting lower bound on the dark matter mass in the field of view. The distance to NGC 4123 is approximately 22.4 Mpc. The form of the NFW profile used is the two-parameter spherical density distribution:

$$\rho_{\rm NFW} = \rho_s \frac{4r_s^3}{r(r + r_s)^2} . \quad (26)$$

The halo parameters are from Weiner et al. (2001) and are given in Table 2. The possible limit from a 36 ks exposure (see eq. [15]) is $m_s \lesssim 10.3$ keV in the $L_{\nu_\alpha} \approx 0$ production mode case.

We also use the rotation curve of NGC 3198 (van Albada et al. 1985) to fit an NFW profile for the dark matter in this object. We use a mass-to-light ratio of unity, which provides a good fit for the inner part of the rotation curve. The halo parameters are given in Table 2. We adopt a distance of 18.34 Mpc to NGC 3198, from Willick & Batra (2001). The potential mass limit (eq. [15]) for a 36 ks observation in this case is $m_s \lesssim 6.0$ keV for the $L_{\nu_\alpha} \approx 0$ models.

In Figure 4 we show the detectability region for observations of NGC 3198 with Constellation X—a proposed fleet of observatories that will have an effective area ~ 10 times greater than *Chandra* and no instrumental background (Valinia et al. 1999)—for two integration times, 1 and 10 Ms, which conceivably could be achieved through several long observations over a few years. An exposure equivalent to this could be obtained by a stacking analysis of the spectra of a number of similar clusters (see, e.g., Brandt et al. 2001; Tozzi et al. 2001). Constellation X, with very long integration times, holds out the prospect of covering nearly the entire WDM parameter space of interest for

TABLE 2

FIELD GALAXIES

Name	ρ_s ($\times 10^{14}\ M_\odot$ Mpc^{-3})	r_s (kpc)	$M(<r_s)$ ($\times 10^{11}\ M_\odot$)	$M_{\rm DM}^{\rm fov}$[a] ($\times 10^{11}\ M_\odot$)	Γ Limit[b] (yr^{-1})	$m_s(L_{\nu_\alpha} \approx 0)$ Limit[c] (keV)
NGC 3198.....	1.5	67.0	4.32	3.62	$(2.3 \times 10^{18})^{-1}$	6.0
NGC 4123.....	1.3	38.2	0.704	1.85	$(2.3 \times 10^{17})^{-1}$	10.3

[a] The mass within the field of view $M_{\rm DM}^{\rm fov}$ (density integrated over the rectangular prism in the field of view).
[b] The potential limit on the radiative decay rate Γ_γ of dark matter from the object with a 36 ks observation.
[c] The corresponding constraint on the singlet neutrino mass, m_s, in the $L_{\nu_\alpha} \approx 0$ case (eq. [15]).

some of the resonant production mode scenarios up to lepton number $L \lesssim 0.1$.

We should note, however, that it is still uncertain how low in m_s (i.e., X-ray photon line energy) Constellation X can be sensitive to at the limiting X-ray flux given in Figure 4 (10^{-19} ergs cm^{-2} s^{-1}). In fact, it could be that the lowest photon energy detectable on Constellation X could be between 0.3 and 0.5 keV. We show the possible constraint with detectability down to 0.3 keV photons, or $m_s \approx 0.6$ keV. As described in the introduction, Lyα forest considerations disfavor $m_s \lesssim 2.0$ keV, and therefore Constellation X in principle can detect/exclude essentially all of the remaining singlet neutrino parameter space for $L_{\nu_\alpha} \lesssim 0.1$.

5. DIFFUSE PHOTON LIMITS

The flux per unit energy per unit solid angle from a homogeneously distributed decaying background dark matter particle is (Massó & Toldrà 1999)

$$\frac{d^2F}{dE_\gamma\, d\Omega} = \frac{\Gamma_\gamma}{4\pi}\frac{\tilde{n}_{\nu_s}(t_0)}{H(z_0)}\, e^{-\Gamma_{\rm tot}\, t(z_0)}\,, \tag{27}$$

where $\tilde{n}_{\nu_s}(t_0)$ is the present number density of dark matter if it did not decay, $\Gamma_{\rm tot}$ is the total decay rate of the particle, z_0 is the redshift at which the photon was produced, and $t(z_0)$ is the age of the universe at z_0. A photon that has present energy E_γ was produced at redshift z_0 given by

$$1 + z_0 = \frac{m_s/2}{E_\gamma}\,. \tag{28}$$

Limits on the diffuse extragalactic background radiation (DEBRA; sometimes referred to as extragalactic background light [EBL]) can be used to constrain dark matter particles that produce a flux given by equation (27). Diffuse radiative decay constraints also were emphasized by Drees (2000) and Drees & Wright (2000) in papers that incorrectly estimate the relic density of singlet neutrinos (see Dodelson & Widrow 1994; Dolgov & Hansen 2000; AFP). A broadband limit was placed by Ressell & Turner (1989) on DEBRA. They found that the flux per unit solid angle must satisfy

$$d\mathscr{F}/d\Omega \lesssim (1\ {\rm MeV}/E_\gamma)\ {\rm cm}^{-2}\ {\rm sr}^{-1}\ {\rm s}^{-1}\,. \tag{29}$$

Shown in Figure 6 are these less constraining, yet broadband, bounds from Ressell & Turner (1989) for the $L_{\nu_\alpha} \approx 0$ case for singlet neutrino WDM.

Gruber (1992) found the form of the X-ray background to be

$$\frac{d\mathscr{F}}{d\Omega} \lesssim 7.9\ {\rm cm}^{-2}\ {\rm sr}^{-1}\ {\rm s}^{-1}\left(\frac{E_\gamma}{\rm keV}\right)^{-0.29} e^{-(E_\gamma/41\ {\rm keV})} \tag{30}$$

for energies of $\sim$3–60 keV and

$$\frac{d\mathscr{F}}{d\Omega} \lesssim 1650\ {\rm cm}^{-2}\ {\rm sr}^{-1}\ {\rm s}^{-1}\left(\frac{E_\gamma}{\rm keV}\right)^{-2.0} + 1750\ {\rm cm}^{-2}\ {\rm sr}^{-1}\ {\rm s}^{-1}\left(\frac{E_\gamma}{\rm keV}\right)^{-0.7} \tag{31}$$

from 60 keV to $\sim$6 MeV. These constraints are also shown in Figure 6 for the $L_{\nu_\alpha} \approx 0$ singlet WDM case.

Recently, the *Chandra X-Ray Observatory* (Hornschmeier et al. 2001; Tozzi et al. 2001) has resolved several structures that contributed to the unresolved X-ray background. They find that the resolved sources contributed from 60% to 90% of the previously unresolved background. We make a rough approximation from these considerations that at most $\sim$20% of the X-ray background described by Gruber (1992) may be due to a diffuse particle decay. The limits from this consideration are depicted in Figure 6 for the $L_{\nu_\alpha} \approx 0$ case.

However, these diffuse limits entail the implicit assumption that dark matter particles are not concentrated in objects but rather are *uniformly* distributed through space. This is certainly not the case, since structure has been at least somewhat clumped and nonisotropic in the sky since an epoch corresponding to a redshift of $z \gtrsim 10$. The limits on the singlet neutrino mass in the $L_{\nu_\alpha} \approx 0$ case obtained by

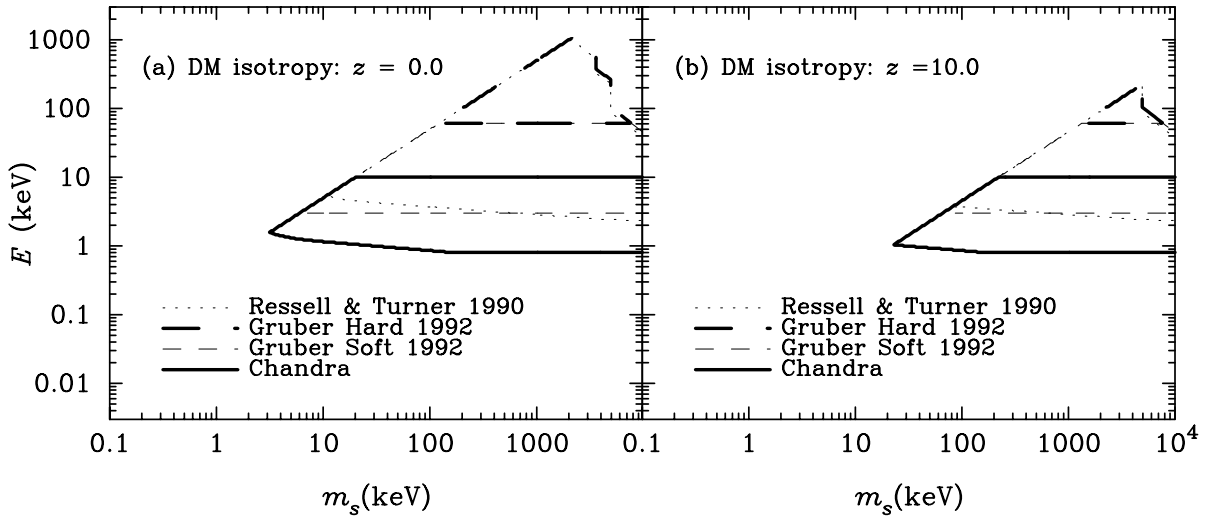

FIG. 6.—Limits on the diffuse flux from singlet neutrino decay in the $L_{\nu_\alpha} \approx 0$ case from photons produced at (*a*) $z \geq 0$ and (*b*) $z \geq 10$, assuming isotropy of the dark matter at that redshift.

an assumption of no clumping right up to the present ($z = 0$) epoch are shown in Figure 6*a*. This limit is roughly $m_s \lesssim 2$ keV. The limits for singlet dark matter in the $L_{\nu_\alpha} \approx 0$ case decaying at $z \gtrsim 10$, shown in Figure 6*b*, is approximately $m_s \lesssim 20$ keV. In this case the diffuse limit is greatly eased for the obvious reason that there is little diffuse dark matter at recent epochs. The true limit from a diffuse component should lie between these extreme cases. The actual limit depends on the epoch of significant structure formation and therefore on particular structure formation models.

6. CONCLUSIONS

We have argued that the serendipitous coincidence between the "sweet spot" for X-ray photon detection technology (photon energies between 0.5 and 10 keV on modern observatories like *Chandra* and *XMM-Newton*) and the structure consideration–preferred WDM particle rest mass range may afford an opportunity to detect or exclude a number of WDM candidates. Present observations of X-ray emission from clusters of galaxies (e.g., Virgo) may already nearly eliminate all but a small parameter region for the zero lepton number, nonresonant scattering production mode for singlet "sterile" neutrino WDM. We find that the nonobservance of a significant feature in deep observations of the central region of the Virgo Cluster excludes singlet neutrino WDM candidates with masses $m_s \gtrsim 5$ keV in the $L_{\nu_\alpha} \approx 0$ production mode.

However, exposures of large dark matter halos by current X-ray observatories could yield a spectral line for 2.5 keV $\lesssim m_s \lesssim 5$ keV (1.25 keV $\lesssim E_\gamma \lesssim 2.5$ keV) in the $L_{\nu_\alpha} \approx 0$ case unassociated with any atomic line. As detailed observations of the spatially resolved gas temperature profiles of rich clusters continue, accurate determinations of the dark matter profile in these clusters can be made, and existing limits and their uncertainties can be improved. Combined with lower mass bounds, upper limits from observation may exclude certain dark matter particle candidates.

The best strategy would be to target hot clusters or halos of spiral galaxies, which should have few emission lines in the energy range 1.25 keV $\lesssim E_\gamma \lesssim 2.5$ keV. In addition, the inferred existence of weakly lensing dark massive "blobs" (Clowe et al. 2001) provides a candidate for dark matter decay photon detection with relatively no background; however, the distance to such dark lenses is not well known, and therefore constraints on dark matter particle decay cannot be established from these objects.

The remaining (undetectable with ACIS on *Chandra*) $L_{\nu_\alpha} \approx 0$ parameter region is centered on $m_s \sim 1$ keV, the most interesting rest mass from a structure formation standpoint. Though this parameter space is already challenged by potential supernova core cooling effects (see, e.g., AFP), it would still be useful to close this window with another constraint venue.

The nonzero lepton number ($L_{\nu_\alpha} \neq 0$) cases for singlet neutrino WDM, corresponding to resonant production in the early universe (Shi & Fuller 1999; AFP) are not as yet detectable or constrainable with *Chandra*/*XMM*. However, the higher sensitivities that are possible with the Constellation X observatory could cover much of the interesting parameter space for these singlet neutrino models.

This is an exciting possibility. A line feature not attributable to an atomic line could be produced by the radiative decay of either singlet neutrinos, heavy active neutrinos, or gravitinos.

In any case, it is remarkable and unexpected that the hard-won technology of X-ray astronomy can in some cases probe a new regime of particle physics, one where particle interaction strengths are some 10 orders of magnitude weaker than the weak interaction. Put another way, modern X-ray observatories could probe epochs of the early universe corresponding to redshifts $z \sim 10^{12}$.

We would like to thank A. B. Balantekin, J. Bookbinder, D. O. Caldwell, G. Fossati, W. Heindl, M. Patel, R. Rothschild, and J. Tomsick for useful discussions. We would like to thank N. Dalal for suggesting nonluminous massive gravitational lenses as dark matter sources. This work was supported in part by NSF grant PHY 98-00980 at UCSD. K. A. would like to acknowledge support from a NASA GSRP fellowship. W. T. was supported in part by NASA contract NAS8-39073.

REFERENCES

Abazajian, K., Fuller, G. M., & Patel, M. 2001, Phys. Rev. D, 64, 023501 (AFP)
Abel, T., Anninos, P., Norman, M. L., & Zhang, Y. 1998, ApJ, 508, 518
Arkani-Hamed, N., Dimopoulos, S., & Dvali, G. 1998, Phys. Lett. B, 429, 263
Barger, V., Phillips, R. J. N., & Sarkar, S. 1995, Phys. Lett. B, 352, 365
Barkana, R., Haiman, Z., & Ostriker, J. P. 2001, ApJ, 558, 482
Binney, J., Gerhard, O., & Silk, J. 2001, MNRAS, 321, 471
Bode, P., Ostriker, J. P., & Turok, N. 2001, ApJ, 556, 93
Boehm, F., & Vogel, P. 1987, Physics of Massive Neutrinos (Cambridge: Cambridge Univ. Press)
Böhringer, H., et al. 2001, A&A, 365, L181
Brandt, N., et al. 2001, AJ, 122, 1
Bullock, J. S., Kravtsov, A. V., & Weinberg, D. H. 2001, ApJ, 548, 33
Caldwell, D. O. 1998, Int. J. Mod. Phys. A, 13, 4409
Cavaliere, A., & Fusco-Femiano, R. 1978, A&A, 70, 677
Clowe, D., Luppino, G., Kaiser, N., & Gioia, I. 2001, ApJ, 539, 540
Colombi, S., Dodelson, S., & Widrow, L. M. 1996, ApJ, 458, 1
Cowsik, R., & McClelland, J. 1972, Phys. Rev. Lett., 29, 669
Dalcanton, J. J., & Hogan, C. J. 2001, ApJ, 561, 35
Dicus, D. A., Kolb, E. W., & Teplitz, V. L. 1978, ApJ, 221, 327
Dine, M., Nelson, A. E., Nir, Y., & Shirman, Y. 1996, Phys. Rev. D, 53, 2658
Dodelson, S., & Widrow, L. M. 1994, Phys. Rev. Lett., 72, 17
Dolgov, A. D., & Hansen, S. H. 2000, preprint (hep-ph/0009083)
Drees, M. 2000, preprint (hep-ph/0003127)
Drees, M., & Wright, D. 2000, preprint (hep-ph/0006274)
Einasto, J., Kaasik, A., & Saar, E. 1974, Nature, 250, 309
Federspiel, M., Tammann, G. A., & Sandage, A. 1998, ApJ, 495, 115
Gerstein, S. S., & Zeldovich, Ya. B. 1966, Zh. Eksp. Teor. Fiz., 4, 174
Ghigna, S., Moore, B., Governato, F., Lake, G., Quinn, T., & Stadel, J. 2000, ApJ, 544, 616
Giudice, G. F., Kolb, E. W., & Riotto, A. 2001a, Phys. Rev. D, 64, 023508
Giudice, G. F., Kolb, E. W., Riotto, A., Semikoz, D. V., & Tkachev, I. I. 2001b, Phys. Rev. D, 64, 043512
Groom, D. E., et al. 2000, European Phys. J. C, 15, 1
Gruber, D. E. 1992, in The X-Ray Background, ed. X. Barcons & A. C. Fabian (Cambridge: Cambridge Univ. Press), 44
Hall, L. J., & Suzuki, M. 1984, Nucl. Phys. B, 231, 419
Horner, D. J., Mushotzky, R. F., & Scharf, C. A. 1999, ApJ, 520, 78
Hornschmeier, A. E., et al. 2001, ApJ, 554, 742
Kawasaki, M., Kohri, K., & Sugiyama, N. 2000, Phys. Rev. D, 62, 023506
Kawasaki, M., Sugiyama, N., & Yanagida, T. 1997, Mod. Phys. Lett. A, 12, 1275
Massó, E., & Toldrà, R. 1999, Phys. Rev. D, 60, 083503
Melott, A. L., Splinter, R. J., Persic, M., & Salucci, P. 1994, ApJ, 421, 16
Mikheyev, S. P., & Smirnov, A. Y. 1985, Soviet J. Nucl. Phys., 24, 913
Moore, B., Ghigna, S., Governato, F., Lake, G., Quinn, T., Stadel, J., & Tozzi, P. 1999, ApJ, 524, L19
Narayanan, V. K., Spergel, D. N., Davé, R., & Ma, C. 2000, ApJ, 543, L103
Navarro, J. F., Frenk, C. S., & White, S. D. M. 1995, MNRAS, 275, 720
———. 1996, ApJ, 462, 563
Nieves, J. F. 1983, Phys. Rev. D, 28, 1664
Ostriker, J. P., Peebles, P. J. E., & Yahil, A. 1974, ApJ, 193, L1
Pal, P. B., & Wolfenstein, L. 1982, Phys. Rev. D, 25, 766
Qian, Y., & Wasserburg, G. J. 2001, ApJ, 549, 337

Ressell, M. T., & Turner, M. S. 1989, Comments Astrophys., 14, 323
Sciama, D. W. 1990, ApJ, 364, 549
Sellwood, J. A. 2000, ApJ, 540, L1
Shi, X., & Fuller, G. M. 1999, Phys. Rev. Lett., 82, 2832
Shipman, H. L., & Cowsik, R. 1981, ApJ, 247, L111
Spergel, D. N., & Steinhardt, P. J. 2000, Phys. Rev. Lett., 84, 3760
Swaters, R. A., Madore, B. F., & Trewhella, M. 2000, ApJ, 531, L107
Takayama, F., & Yamaguchi, M. 2000, Phys. Lett. B, 485, 388
Tozzi, P., et al. 2001, ApJ, in press (astro-ph/0103014)
Valinia, A., et al. (The Constellation X Team). 1999, in AIP Conf. Proc. 470, After the Dark Ages: When Galaxies Were Young (the Universe at $2 < z < 5$): Ninth Astrophysics Conference, ed. S. S. Holt & E. P. Smith (Woodbury: AIP), 434
van Albada, T. S., Bahcall, J. N., Begeman, K., & Sancisi, R. 1985, ApJ, 295, 305
van den Bosch, F. C., Robertson, B. E., Dalcanton, J. J., & de Blok, W. J. G. 2000, AJ, 119, 1579
Weiner, B. J., Williams, T. B., van Gorkom, J. H., & Sellwood, J. A. 2001, ApJ, 546, 916
Willick, J. A., & Batra, P. 2001, ApJ, 548, 564
Wolfenstein, L. 1978, Phys. Rev. D, 17, 2369
Zwicky, F. 1933, Helvetica Phys. Acta, 6, 110

Note added in proof.—It should be noted that the three-neurtino decay processes of the singlet neutrino in Figure 1 (with the rate of eq. [7]) are possible only in the presence of a flavor-changing neutral current between neutrino flavors. We thank John Beacom for suggesting a clarification and emphasis of this point.